

1 **Neutralizing antibody and soluble ACE2 inhibition of a replication-competent VSV-**
2 **SARS-CoV-2 and a clinical isolate of SARS-CoV-2.**

3
4 James Brett Case^{1*}, Paul W. Rothlauf^{2,6*}, Rita E. Chen^{1,3}, Zhuoming Liu², Haiyan Zhao⁴, Arthur
5 S. Kim^{1,3}, Louis-Marie Bloyet², Qiru Zeng², Stephen Tahan², Lindsay Droit², Ma. Xenia G. Ilagan⁴,
6 Michael A. Tartell^{2,6}, Gaya Amarasinghe^{2,3,4}, Jeffrey P. Henderson¹, Shane Miersch⁷, Mart Ustav⁷,
7 Sachdev Sidhu⁷, Herbert W. Virgin⁸, David Wang², Siyuan Ding², Davide Corti⁹, Elitza S. Theel¹⁰,
8 Daved H. Fremont^{2,3,4,5}, Michael S. Diamond^{1,2,4,5}‡ and Sean P.J. Whelan²‡,

9
10 Department of Medicine¹, Molecular Microbiology², Pathology & Immunology³, Biochemistry &
11 Molecular Biophysics⁴ and The Andrew M. and Jane M. Bursky Center for Human Immunology &
12 Immunotherapy Programs⁵, Washington University School of Medicine, St. Louis, MO, USA.

13 ⁶Program in Virology, Harvard Medical School, Boston, MA, USA. ⁷The Donnelly Centre,
14 University of Toronto, Toronto, Canada. ⁸Vir Biotechnology, San Francisco, CA, USA. ⁹Humabs
15 BioMed SA, a subsidiary of Vir Biotechnology, Inc., CH-6500, Bellinzona, Switzerland. ¹⁰Division
16 of Clinical Microbiology, Department of Laboratory Medicine and Pathology, Mayo Clinic,
17 Rochester, MN, USA

18
19 * Equal contributors

20 ‡ **Corresponding authors:** Sean P.J. Whelan Ph.D., spjwhelan@wustl.edu and Michael S.
21 Diamond, M.D., Ph.D., diamond@wusm.wustl.edu;

22
23 **Figures: 5**

25 **ABSTRACT**

26 Antibody-based interventions against SARS-CoV-2 could limit morbidity, mortality, and
27 possibly disrupt epidemic transmission. An anticipated correlate of such countermeasures is the
28 level of neutralizing antibodies against the SARS-CoV-2 spike protein, yet there is no consensus
29 as to which assay should be used for such measurements. Using an infectious molecular clone
30 of vesicular stomatitis virus (VSV) that expresses eGFP as a marker of infection, we replaced the
31 glycoprotein gene (G) with the spike protein of SARS-CoV-2 (VSV-eGFP-SARS-CoV-2) and
32 developed a high-throughput imaging-based neutralization assay at biosafety level 2. We also
33 developed a focus reduction neutralization test with a clinical isolate of SARS-CoV-2 at biosafety
34 level 3. We compared the neutralizing activities of monoclonal and polyclonal antibody
35 preparations, as well as ACE2-Fc soluble decoy protein in both assays and find an exceptionally
36 high degree of concordance. The two assays will help define correlates of protection for antibody-
37 based countermeasures including therapeutic antibodies, immune γ -globulin or plasma
38 preparations, and vaccines against SARS-CoV-2. Replication-competent VSV-eGFP-SARS-
39 CoV-2 provides a rapid assay for testing inhibitors of SARS-CoV-2 mediated entry that can be
40 performed in 7.5 hours under reduced biosafety containment.

41

42 INTRODUCTION

43 Severe acute respiratory syndrome coronavirus 2 (SARS-CoV-2) is a positive-sense,
44 single-stranded, enveloped RNA virus that was first isolated in Wuhan, China in December, 2019
45 from a cluster of acute respiratory illness cases (Guan et al., 2020). SARS-CoV-2 is the etiologic
46 agent of coronavirus disease 2019 (COVID-19), which as of May 16, 2020 has more than 4.5
47 million confirmed cases causing 309,000 deaths. Virtually all countries and territories have been
48 affected, with major epidemics in Central China, Italy, Spain, France, Iran, Russia, the United
49 Kingdom, and the United States. SARS-CoV-2 is thought to be of zoonotic origin and is closely
50 related to the original SARS-CoV (Zhang et al., 2020; Zhou et al., 2020). Most cases are spread
51 by direct human-to-human transmission, with community transmission occurring from both
52 symptomatic and asymptomatic individuals (Bai et al., 2020). This has resulted in a global
53 pandemic with severe economic, political, and social consequences. The development,
54 characterization, and deployment of an effective vaccine or antibody prophylaxis or treatment
55 against SARS-CoV-2 could prevent morbidity and mortality and curtail its epidemic spread.

56 The viral spike protein (S) mediates all steps of coronavirus entry into target cells including
57 receptor binding and membrane fusion (Tortorici and Veesler, 2019). During viral biogenesis the
58 S protein undergoes furin-dependent proteolytic processing as it transits through the trans-Golgi
59 network and is cleaved into S1 and S2 subunits that function in receptor binding and membrane
60 fusion, respectively (Walls et al., 2020). Angiotensin-converting enzyme 2 (ACE2) serves as a
61 cell surface receptor (Letko et al., 2020; Wrapp et al., 2020) for SARS-CoV-2, and productive
62 infection is facilitated by additional processing of S2 by the host cell serine protease TMPRSS2
63 (Hoffmann et al., 2020).

64 Laboratory studies of SARS-CoV-2 require biosafety level 3 (BSL3) containment with
65 positive-pressure respirators. Single-round pseudotyped viruses complemented by expression of
66 the SARS-CoV-2 S protein *in trans* serve as biosafety level 2 (BSL2) surrogates that can facilitate
67 studies of viral entry, and the inhibition of infection by neutralizing antibodies and other inhibitors

68 (Hoffmann et al., 2020; Lei et al., 2020; Ou et al., 2020). Such pseudotyping approaches are used
69 routinely by many laboratories for other highly pathogenic coronaviruses including SARS-CoV
70 and MERS-CoV (Fukushi et al., 2006; Fukushi et al., 2005; Giroglou et al., 2004; Kobinger et al.,
71 2007). Viral pseudotyping assays are limited by the need to express the glycoprotein *in trans* and
72 preclude forward genetic studies of the viral envelope protein. Expression of the glycoprotein is
73 often accomplished by plasmid transfection, which requires optimization to minimize batch
74 variation. Assays performed with such pseudotyped viruses rely on relative levels of infectivity as
75 measured by a reporter assay without correlation to an infectious titer. It also is unknown as to
76 how the display of S proteins on a heterologous virus impacts viral entry, antibody recognition,
77 and antibody neutralization compared to infectious coronavirus. This question is important
78 because neutralization assays are used to establish correlates of protection for vaccine and
79 antibody-based countermeasures, and most manufacturers lack access to high-containment
80 laboratories to test antibody responses against highly pathogenic coronaviruses including SARS-
81 CoV-2.

82 Here, we developed a simple and robust BSL2 assay for evaluating SARS-CoV-2 entry
83 and its inhibition by antibodies. We engineered an infectious molecular clone of vesicular
84 stomatitis virus (VSV) to encode the SARS-CoV-2 S protein in place of the native envelope
85 glycoprotein (G) and rescued an autonomously replication-competent virus bearing the spike.
86 Through passage of VSV-eGFP-SARS-CoV-2, we selected a gain-of-function mutation in S that
87 allowed more efficient viral propagation yielding titers of $> 1 \times 10^8$ plaque-forming units (PFU)/ml.
88 We characterized this variant with respect to inhibition by soluble human ACE2-Fc and
89 monoclonal and polyclonal antibodies from humans and compared those results to neutralization
90 tests with a clinical isolate of SARS-CoV-2. These studies demonstrate that a recombinant VSV
91 expressing SARS-CoV-2 S behaves analogously to a clinical isolate of SARS-CoV-2, providing a
92 useful high-throughput BSL2 assay for studying antibody neutralization or inhibition of viral spike-
93 mediated entry.

94 **RESULTS**

95 **A replication-competent, infectious VSV chimera with SARS-CoV-2 S protein.** To
96 generate a replication-competent virus to study entry and neutralization of SARS-CoV-2 at BSL2,
97 we engineered an infectious molecular clone of VSV by replacing the endogenous glycoprotein
98 (G) with SARS-CoV-2 S (**Fig 1A**). SARS-CoV-2 S protein contains an endoplasmic reticulum (ER)
99 retention sequence in the cytoplasmic tail (KxHxx-COOH) because virion assembly occurs in ER-
100 Golgi intermediate compartments (Lontok et al., 2004; McBride et al., 2007; Ruch and Machamer,
101 2012). We preemptively altered that sequence to AxAxx to facilitate retargeting of S to the plasma
102 membrane, the site of VSV assembly. Using established approaches (**Fig S1A**) (Whelan et al.,
103 1995), we recovered infectious VSV-eGFP-SARS-CoV-2-S_{AA} as determined by expression of the
104 virus-encoded eGFP reporter (**Fig 1A, right panel**). VSV-eGFP-SARS-CoV-2-S_{AA} propagation
105 was inefficient on Vero CCL81 cells. This result prompted us to test additional modifications of
106 the cytoplasmic tail of S, which were also defective in autonomous amplification (**Fig S1B**). To
107 overcome this limitation, we used a forward genetic approach to isolate an adaptive variant of
108 VSV-eGFP-SARS-CoV-2-S_{AA} (**Fig S1C**). Repeated passage and plaque isolation on Vero CCL81
109 cells led to the emergence of a virus that contained a cysteine to stop mutation at residue 1253
110 (TGC to TGA at nucleotide 3759), which truncates the cytoplasmic tail of SARS-CoV-2 S by 21
111 residues (**Fig 1A**). We confirmed that this was the only mutation in the viral genome by next
112 generation sequencing (Supplemental Data). Comparison of plaque morphology of VSV-eGFP-
113 SARS-CoV-2-S_{Δ21} and VSV-eGFP-SARS-CoV-2-S_{AA} on three Vero cell subtypes and an
114 additional rhesus monkey cell line (MA104) demonstrates that the selected variant spreads more
115 efficiently (**Fig 1B**). Screening of a larger panel of cell types (**Fig 1C**) identified MA104 and Vero
116 E6 cells as supporting the highest levels of virus production. Ectopic expression of TMPRSS2 led
117 to a further ~10-fold increase in viral titer and a larger plaque size (**Fig 1D**).

118 **SARS-CoV-2-S_{Δ21} is incorporated into infectious VSV particles.** To confirm
119 incorporation of SARS-CoV-2 S into particles, we first amplified the virus in the presence of VSV

120 G to allow infection of cell types independently of the S protein. The VSV G *trans*-complemented
121 VSV-SARS-CoV-2-S_{Δ21} efficiently infects HEK293T cells, which then serve as a source of
122 production of virus particles containing SARS-CoV-2 S protein. Western blotting of supernatants
123 with CR3022, a cross-reactive anti-S monoclonal antibody (mAb) (ter Meulen et al., 2006; Yuan
124 et al., 2020), established the presence of S_{Δ21} in VSV-SARS-CoV-2-S_{Δ21} particles but not in the
125 parental VSV (**Fig 1E**). The protein detected migrated at ~100 kilodaltons, a band that
126 corresponds to the cleaved S1 subunit of the glycoprotein (Watanabe et al., 2020). To examine
127 whether the S_{Δ21} incorporated into VSV particles is processed to S1 and S2, we performed [³⁵S]
128 cysteine-methionine metabolic labeling in BSRT7 cells, which support robust VSV replication, and
129 analyzed released particles by SDS-PAGE and phosphorimaging. In addition to the VSV
130 structural proteins (N, P, M and L), two additional bands were observed for VSV-SARS-CoV-2-
131 S_{Δ21} that correspond in size to glycosylated S1 (107 kDa) and S2_{Δ21} (85 kDa) (**Fig 1F**). Negative-
132 stain electron microscopy of sucrose-gradient purified virus particles revealed that the membrane
133 protein projecting from VSV-SARS-CoV-2-S_{Δ21} is larger than observed on wild-type VSV particles
134 (**Fig 1G**), which reflects the larger size of the coronavirus spike.

135 **A high-throughput focus-forming assay with a clinical isolate of SARS-CoV-2.** VSV-
136 SARS-CoV-2-S_{Δ21} has several advantages for detection and measuring of neutralizing antibodies,
137 including lower biosafety containment level, ease of production and use, and rapid reporter gene
138 readout. Nonetheless, the difference in virus morphology (spherical CoV versus bullet-shaped
139 VSV) and possible effects on the conformational display of S on the virion surface, raise questions
140 as to whether the accessibility of epitopes and stoichiometry of antibody neutralization is similar
141 to authentic SARS-CoV-2. A direct comparison with a clinical isolate of SARS-CoV-2 is necessary
142 to establish the utility of VSV-SARS-CoV-2-S_{Δ21} for assays of viral entry and antibody
143 neutralization.

144 We designed a high-throughput assay for titrating SARS-CoV-2 that could be applied to
145 multiple cell substrates. Instead of using a plaque assay, which relies on the capacity for a virus

146 to cause cell death, which can vary across cell types, we developed a focus-forming assay (FFA)
147 and viral antigen detection as a measure of infectivity. We propagated SARS-CoV-2 in four
148 different producer cell types (Vero CCL81, Vero E6, Vero-furin, and MA104 cells) and then
149 measured the number and size of foci after staining recipient cells with an anti-S mAb. With SARS-
150 CoV-2 stocks generated from each producer cell type, we observed distinct foci across recipient
151 cell substrates at approximately 30 h post-inoculation (**Fig 2A**). We consistently observed the
152 highest viral titers and largest foci sizes with Vero-furin and MA104 cells (**Fig 2B-C**). However,
153 the larger foci were more difficult to enumerate on an automated Immunospot reader and required
154 additional manual quality control analysis. Because of this, we used Vero E6 cells for our rapid
155 focus-reduction neutralization tests (FRNT) in subsequent experiments.

156 **A high-throughput, eGFP-based neutralization assay for VSV-SARS-CoV-2-S_{Δ21}.** In
157 parallel, we developed a high-throughput method to measure neutralization of VSV-SARS-CoV-
158 2-S_{Δ21}. As VSV-SARS-CoV-2-S_{Δ21} encodes an eGFP reporter and viral gene expression is robust,
159 eGFP-positive cells can be quantified 7.5 h post-infection using a fluorescence microscope with
160 automated counting analysis software. This approach enabled the development of an eGFP-
161 reduction neutralization test (GRNT) (**Fig 2D**).

162 **Neutralization of VSV-SARS-CoV-2-S_{Δ21} and SARS-CoV-2 by human antibodies.**
163 Members of our group recently identified human mAbs from memory B cells of a SARS-CoV
164 survivor that bind to SARS-CoV-2 S (Pinto et al, 2020). We tested a subset of these (mAbs 304,
165 306, 309, and 315) for their ability to inhibit VSV-SARS-CoV-2-S_{Δ21} and SARS-CoV-2 infections
166 on Vero E6 cells. While three of these mAbs showed poor inhibitory activity, mAb 309 potently
167 neutralized both SARS-CoV-2 and VSV-SARS-CoV-2-S_{Δ21} (**Fig 3A-B**) with similar EC₅₀ values
168 between the two assays (81 and 67 ng/mL for SARS-CoV-2 and VSV-SARS-CoV-2-S_{Δ21},
169 respectively). To broaden the test panel, we evaluated the activity of a panel of mAbs generated
170 as part of a phage display library (Sachev Sidhu, unpublished data) by both FRNT and GRNT.
171 Many of these mAbs exhibited moderate neutralization activities in the EC₅₀ range of 100 to 500

172 ng/mL (**Fig 3C-D**). Nonetheless, we observed the same neutralization trend between VSV-SARS-
173 CoV-2-S_{Δ21} and SARS-CoV-2 with highly correlated EC₅₀ values (< 2-fold differences).

174 **Neutralization by human ACE2-Fc receptor decoy proteins.** Human ACE2 (hACE2) is
175 an entry receptor for both SARS-CoV and SARS-CoV-2 (Letko et al., 2020; Li et al., 2005; Li et
176 al., 2003; Wrapp et al., 2020). As a soluble hACE2-Fc decoy protein has been proposed as a
177 therapeutic for SARS-CoV-2 (Kruse, 2020), in part based on its ability to inhibit SARS-CoV
178 infection in cell culture (Moore et al., 2004), we tested whether hACE2-Fc could inhibit infection
179 of VSV-SARS-CoV-2-S_{Δ21} and SARS-CoV-2 using our FRNT and GRNT assays. When pre-mixed
180 with VSV-SARS-CoV-2-S_{Δ21} or SARS-CoV-2, hACE2-Fc, but not murine ACE2-Fc (mACE2-Fc),
181 dose-dependently and equivalently inhibited infection of recipient Vero E6 cells (**Fig 3E-F**). As
182 expected, hACE2-Fc did not inhibit infection of wild-type VSV confirming that neutralization was
183 specific to the SARS-CoV-2 S protein (**Fig S2**). We noted a relatively high concentration of
184 hACE2-Fc was required for inhibition with EC₅₀ values of 29 and 12.6 μg/ml for VSV-SARS-CoV-
185 2-S_{Δ21} and SARS-CoV-2, respectively. Thus, although soluble hACE2-Fc decoy proteins similarly
186 inhibit infection of VSV-SARS-CoV-2-S_{Δ21} and SARS-CoV-2, the potency is less than anticipated,
187 which suggests that the receptor-binding domain (RBD) on the S protein on the surface of both
188 viruses may not be fully accessible in solution.

189 **Neutralization of VSV-SARS-CoV-2-S_{Δ21} and SARS-CoV-2 by human immune serum.**

190 As part of studies to evaluate immune convalescent plasma as a possible therapy for SARS-CoV-
191 2 infected patients (Bloch et al., 2020), we obtained 42 serum samples from 20 individuals at
192 different time points after the onset of COVID-19 symptoms (**Table 1**). These samples were pre-
193 screened using a commercially available IgG ELISA. We tested each sample for neutralization of
194 VSV-SARS-CoV-2-S_{Δ21} and SARS-CoV-2 on Vero E6 cells. We observed that sera with ELISA
195 negative or indeterminate results generally showed low inhibitory titers (EC₅₀ < 1/100), whereas
196 ELISA positive sera generated a broad range of neutralizing antibody activity (EC₅₀ > 1/200 to

197 >1/1,900) (**Fig 4A and C, Fig S3**). Remarkably, neutralization of VSV-SARS-CoV-2-S_{Δ21} and
198 SARS-CoV-2 was similar across the entire panel of samples (**Fig 4B and C, Fig S3**).

199 **VSV-SARS-CoV-2-S_{Δ21} and SARS-CoV-2 neutralization assays are highly**
200 **correlative.** We determined the extent to which the VSV-SARS-CoV-2-S_{Δ21} and SARS-CoV-2
201 neutralization tests correlated with each other. We compared the GRNT and FRNT EC₅₀ values
202 obtained in assays with mAbs, polyclonal sera, and soluble ACE2 protein (**Fig 5**). For the samples
203 with neutralizing activity, we observed a remarkably strong correlation between the two assays (r
204 = 0.9285; $p < 0.001$). Moreover, all 11 of the samples that were deemed non-neutralizing in one
205 assay had the same result in the second assay. Together, these results establish the utility of
206 using VSV-SARS-CoV-2-S_{Δ21} as a surrogate for authentic SARS-CoV-2 infection in entry
207 inhibition and neutralization studies.

208

209 **DISCUSSION**

210 Emerging viral pathogens have caused numerous epidemics and several pandemics over
211 the last century. The most recent example, SARS-CoV-2, has spread to nearly every country in
212 the world in just a few months, causing millions of infections and hundreds of thousands of deaths
213 (<https://www.worldometers.info/coronavirus/>). Rapid responses to viral outbreaks and generation
214 of countermeasures require readily accessible tools to facilitate study and evaluate antiviral
215 activity. Here, we generated a high-titer, replication-competent chimeric VSV expressing the
216 SARS-CoV-2 S protein that performs similarly to a SARS-CoV-2 clinical isolate across multiple
217 neutralization tests. As access to BSL3 facilities is limited, the finding that VSV-SARS-CoV-2-S Δ ₂₁
218 is neutralized similarly by decoy receptors, mAbs, and polyclonal antibodies in comparison to
219 authentic SARS-CoV-2 is important. This tool will enable academic, government, and industry
220 investigators to rapidly perform assays that interrogate SARS-CoV-2 entry, neutralization, and
221 inhibition at a BSL2 level, which should simplify and expedite the discovery of therapeutic
222 interventions and analysis of functional humoral immune responses.

223 Upon recovery of VSV-SARS-CoV-2-S_{AA}, we selected for a mutant, which contained a 21-
224 amino acid deletion in the cytoplasmic tail. As truncation of the cytoplasmic tail eliminates the
225 modified KxHxx ER retention signal, we suggest that this mutation facilitates more efficient
226 incorporation of the SARS-CoV-2 S protein into the VSV particles. Although truncation of the
227 cytoplasmic tail of HIV envelope protein resulted in conformational alterations in the ectodomain
228 of the protein (Chen et al., 2015), based on the extensive neutralization data presented here
229 including correlation to neutralization of a clinical isolate of SARS CoV-2, a 21-amino acid
230 truncation does not appear to substantively alter the structure of the S protein ectodomain. It
231 remains to be determined whether fully wild-type S protein can incorporate efficiently into VSV.
232 Indeed, similar mutations were generated in the SARS-CoV S protein cytoplasmic tail to boost
233 incorporation into retroviruses and VSV pseudotypes (Fukushi et al., 2005; Giroglou et al., 2004;
234 Moore et al., 2004).

235 The value of a chimeric virus depends on its capacity to present viral surface antigens in
236 a similar way to its authentic counterpart (Garbutt et al., 2004). Indeed, the morphology of the
237 bullet-shaped rhabdovirus and the spherical coronavirus and the density and geometry of S
238 protein display could differentially impact antibody engagement and neutralization. Despite this
239 concern, our extensive testing of VSV-SARS-CoV-2-S_{Δ21} with antibodies and soluble ACE2-Fc
240 proteins showed similar neutralization profiles compared to authentic, fully infectious SARS-CoV-
241 2. Thus, VSV-SARS-CoV-2-S_{Δ21}, despite the structural differences of the virion, provides a useful
242 tool for screening antibodies, entry-based antiviral agents, and vaccine responses against SARS-
243 CoV-2. Indeed, convalescent plasma is under investigation as a potential COVID-19 therapeutic
244 (Chen et al., 2020). Our studies suggest that in addition to testing for anti-S or anti-RBD antibodies
245 (Shen et al., 2020), neutralization assays with VSV-SARS-CoV-2-S_{Δ21} may be a convenient and
246 rapid method to obtain functional information about immune plasma preparations to enable
247 prioritization prior to passive transfer to COVID-19 patients.

248 Coronaviruses possess a roughly 30 kb RNA genome, which requires that they encode a
249 proofreading enzyme (ExoN in nsp14) (Denison et al., 2011) to counteract the error rate of the
250 viral RNA-dependent RNA polymerase. The lack of such proofreading enzymes in the genomes
251 of rhabdoviruses suggests that selection of escape mutants to inhibitors of the coronavirus S
252 protein will be faster in VSV-SARS-CoV-2, which further increases the utility of this chimeric virus.
253 Our FRNT and GRNT assays can be used to establish evidence of prior SARS-CoV-2 infection
254 or vaccination, as well as determine waning of functional responses over time, as the likelihood
255 of cross-neutralizing responses with other cosmopolitan coronaviruses (e.g., HCoV-229E and
256 HCoV-OC43) is exceedingly low. Overall, VSV-SARS-CoV-2-S_{Δ21} and our FRNT and GRNT
257 assays, can facilitate the development and evaluation of antibody- or entry-based
258 countermeasures against SARS-CoV-2 infection.

259

260 **ACKNOWLEDGEMENTS**

261 This study was supported by NIH contracts and grants (75N93019C00062,
262 HHSN272201700060C and R01 AI127828, R37 AI059371 and U01 AI151810) and the Defense
263 Advanced Research Project Agency (HR001117S0019) and gifts from Washington University in
264 Saint Louis. J.B.C. is supported by a Helen Hay Whitney Foundation postdoctoral fellowship. We
265 thank James Rini for providing RBD used to detect phage display mAbs. Some of the figures were
266 created using BioRender.com.

267

268 **AUTHOR CONTRIBUTIONS**

269 J.B.C. performed SARS-CoV-2 neutralization experiments. P.W.R. generated and
270 characterized VSV-SARS-CoV-2-S_{Δ21} and performed neutralization experiments. R.E.C., Z.L.,
271 L.M.B., M.A.T., S.D., and Q.Z. provided experimental assistance. S.T., L.D., and D.W. prepared
272 RNAseq libraries and assembled the VSV-SARS-CoV-2-S_{Δ21} sequence. H.Z. and D.H.F.
273 generated and provided purified proteins, D.C. and H.W.V. provided the recombinant mAbs, S.M.
274 M.U. S.S., and G.A. provided other recombinant mAbs, E.S.T. and J.P.H. identified and provided
275 the human immune serum. M.X.G.I. helped with automated microscope use and analysis. J.B.C,
276 P.W.R., S.P.J.W., and M.S.D. wrote the initial draft, with the other authors providing editing
277 comments.

278

279 **COMPETING FINANCIAL INTERESTS**

280 M.S.D. is a consultant for Inbios, Vir Biotechnology, NGM Biopharmaceuticals, and on the
281 Scientific Advisory Board of Moderna. D.C. and H.W.V. are employees of Vir Biotechnology Inc.
282 and may hold shares in Vir Biotechnology Inc. S.P.J.W. and P.W.R. have filed a disclosure with
283 Washington University for the recombinant VSV.

284

285 **FIGURE LEGENDS**

286 **Figure 1. Generation and characterization of an infectious VSV-SARS-CoV-2**
287 **chimera. (A)** A schematic diagram depicting the genomic organization of the VSV recombinants,
288 shown 3' to 5' are the leader region (Le), eGFP, nucleocapsid (N), phosphoprotein (P), matrix (M),
289 glycoprotein (G) or SARS-CoV-2 S, large polymerase (L), and trailer region (Tr). (*Right panel*)
290 Infection of Vero CCL81 cells with supernatant from cells transfected with the eGFP reporter VSV-
291 SARS-CoV-2-S_{AA}. Images were acquired 44 hours post-infection (hpi) using a fluorescence
292 microscope, and GFP and transmitted light images were merged using ImageJ. (*Bottom panel*)
293 Alignment of the cytoplasmic tail of the VSV-SARS-CoV-2-S_{AA} and the sequence resulting from
294 forward genetic selection of a mutant, which truncated the cytoplasmic tail by 21 amino acids.
295 Mutations deviating from the wild-type spike are indicated in red, and an asterisk signifies a
296 mutation to a stop codon. (**B**) Plaque assays were performed to compare the spread of VSV-
297 SARS-CoV-2-S_{AA} rescue supernatant and VSV-SARS-CoV-2-S_{Δ21} on Vero CCL81, Vero E6,
298 Vero-furin, and MA104 cells. Plates were scanned on a biomolecular imager and expression of
299 eGFP is shown 92 hpi (representative images are shown; n>3 except for S_{AA} on Vero E6, Vero-
300 furin, and MA104 cells). (**C**) The indicated cell types were infected with VSV-SARS-CoV-2-S_{Δ21} at
301 an MOI of 0.5. Cells and supernatants were harvested at 24 hpi and titrated on MA104 cells (data
302 are pooled from three or more independent experiments). (**D**) (*Top panel*) The indicated cells
303 were infected with VSV-SARS-CoV-2-S_{Δ21} at an MOI of 2. Images were acquired 7.5 hpi using a
304 fluorescence microscope and GFP, and transmitted light images were processed and merged
305 using ImageJ (data are representative of two independent experiments). (*Bottom panel*) Plaque
306 assays were performed on the indicated cell types using VSV-SARS-CoV-2-S_{Δ21}. Images showing
307 GFP expression were acquired 48 hpi using a biomolecular imager (data are representative of at
308 least 3 independent experiments). (**E**) Western blotting was performed on concentrated VSV-
309 SARS-CoV-2-S_{Δ21} and wild-type VSV particles on an 8% non-reducing SDS-PAGE gel. S1 was
310 detected using a cross-reactive anti-SARS-CoV mAb (CR3022) (data are representative of two

311 independent experiments). (F) BSRT7/5 cells were inoculated at an MOI of 10 with VSV-eGFP,
312 G-complemented VSV-SARS-CoV-2-S_{Δ21}, or mock infected (not shown), and metabolically
313 labeled with [³⁵S] methionine and cysteine for 20 h starting at 5 hpi in the presence of actinomycin
314 D. Viral supernatants were analyzed by SDS-PAGE. A representative phosphor-image is shown
315 from two independent experiments. An asterisk indicates a band that also was detected in the
316 mock lane (not shown). (G) Purified VSV-WT and VSV-SARS-CoV-2-S_{Δ21} particles were
317 subjected to negative stain electron microscopy. Prefusion structures of each respective
318 glycoprotein are modeled above each EM image (PDB: 5I2S and 6VSB).

319 **Figure 2. Development of a SARS-CoV-2 focus-forming assay and a VSV-SARS-**
320 **CoV-2-S_{Δ21} eGFP-reduction assay.** (A) Representative focus forming assay images of viral
321 stocks generated from each producer cell type (top) were developed on the indicated cell
322 substrates (indicated on the left side). Data are representative of two independent experiments.
323 Foci obtained in (A) were counted (B) and the size was determined (C) using an ImmunoSpot
324 plate reader (* $P < 0.05$, ** $P < 0.01$, *** $P < 0.001$ 1 by One-way ANOVA with Tukey's multiple
325 comparisons test). (D) Representative serial dilution series of VSV-SARS-CoV-2-S_{Δ21} on Vero E6
326 cells. The total number of infected cells per well was quantified using an automated microscope.
327 Insets of enhanced magnification are shown in red. Data are representative of two independent
328 experiments.

329 **Figure 3. Neutralization of VSV-SARS-CoV-2-S_{Δ21} and SARS-CoV-2 by human**
330 **monoclonal antibodies and hACE2 decoy receptors.** A-B. Cross-reactive mAbs isolated from
331 a SARS-CoV survivor were tested for neutralizing activity against SARS-CoV-2 (A) or VSV-
332 SARS-CoV-2-S_{Δ21} (B) (n=2 and 3, respectively). C-D. SARS-CoV-2 RBD-specific antibodies
333 obtained from a phage library were tested for their capacity to neutralize SARS-CoV-2 (C) or VSV-
334 SARS-CoV-2-S_{Δ21} (D) (n=2 and 2, respectively). E-F. hACE2-Fc or mACE2-Fc were tested for
335 their neutralization activity against SARS-CoV-2 (E) or VSV-SARS-CoV-2-S_{Δ21} (F) (n=2 and 3,
336 respectively).

337 **Figure 4. Human immune serum neutralization of SARS-CoV-2 and VSV-SARS-CoV-**
338 **2-S_{Δ21}.** Representative neutralization curves of serum from SARS-CoV-2-infected donors with
339 low, medium, and high inhibitory activity against SARS-CoV-2 (**A**) or VSV-SARS-CoV-2-S_{Δ21} (**B**)
340 (n=2 and 2, respectively). (**C**) EC₅₀ values of all human serum tested for neutralization of SARS-
341 CoV-2 and VSV-SARS-CoV-2-S_{Δ21}. Differences in the geometric mean or median titers were less
342 than 3-fold between FRNT and GRNT assays.

343 **Figure 5. Correlation analysis of neutralization of SARS-CoV-2 and VSV-SARS-CoV-**
344 **2-S_{Δ21}.** EC₅₀ values determined in **Fig 3A-D**, and **4A-B** were used to determine correlation
345 between neutralization assays. Spearman's correlation *r* and *p* values are indicated.

346

347 **SUPPLEMENTARY FIGURE LEGENDS**

348 **Figure S1. Rescue of a chimeric VSV expressing the SARS-CoV-2 S protein and**
349 **forward genetic selection of a gain-of-function mutant.** (**A**) BSRT7/5 cells were infected with
350 vaccinia virus vTF7-3, transfected with plasmids allowing T7-driven expression of VSV N, P, L,
351 and G, and an infectious molecular cDNA of VSV-SARS-CoV-2-S_{AA} to produce replication-
352 competent VSV-SARS-CoV-2-S_{AA}. (**B**) Alignment of the membrane proximal region,
353 transmembrane domain, and cytoplasmic tail of various recombinants that were generated.
354 Successful rescue and indication of spread are noted. (**C**) VSV-SARS-CoV-2-S_{AA} was passaged
355 iteratively on Vero CCL81 cells. Several clones were plaque-purified and amplified on Vero
356 CCL81 cells. RNA from infected cells was extracted and deep sequenced to identify mutants.

357 **Figure S2. Inhibition of VSV-SARS-CoV-2-S_{Δ21} but not VSV with hACE2-Fc receptor**
358 **decoy proteins.** VSV-SARS-CoV-2-S_{Δ21} and VSV were incubated with the indicated human or
359 murine ACE2-Fc receptor decoy proteins, and virus-antibody mixtures were used to infect Vero
360 E6 cells in a GRNT assay. Data are representative of three independent experiments.

361 **Figure S3. Human immune serum neutralization of SARS-CoV-2 and VSV-SARS-**
362 **CoV-2-S_{Δ21}.** As described in **Fig 4**, human serum samples from PCR confirmed SARS-CoV-2-

363 infected patients were tested in FRNT (**A-G**) and GRNT (**H-N**) assays with SARS-CoV-2 and VSV-
364 SARS-CoV-2-S_{Δ21}.
365

366 **METHODS**

367 **Plasmids.** The S gene of SARS-CoV-2 isolate Wuhan-Hu-1 (GenBank MN908947.3) was
368 synthesized in two fragments (Integrated DNA Technologies) and inserted into an infectious
369 molecular clone of VSV (Whelan et al., 1995) as previously (Carette et al., 2011; Jae et al., 2014).
370 Modifications to the cytoplasmic tail were assembled identically. Other plasmids were previously
371 described: VSV N, P, L and G expression plasmids (Stanifer et al., 2011; Whelan et al., 1995),
372 psPAX2 (Addgene), and pLX304-TMPRSS2 (Zang et al., 2020).

373 **Cells.** Cells were maintained in humidified incubators at 34 or 37°C and 5% CO₂ in the
374 indicated media. BSRT7/5, Vero CCL81, Vero E6, Vero E6-TMPRSS2, A549, Caco-2, Caco-2
375 BBe1, Huh7, HepG2, Hela, BHK-21, HEK293, and HEK293T were maintained in DMEM (Corning
376 or VWR) supplemented with glucose, L-glutamine, sodium pyruvate, and 10% fetal bovine serum
377 (FBS). Vero-furin cells (Mukherjee et al., 2016) also were supplemented with 5 µg/ml of blasticidin.
378 MA104 cells were maintained in Medium 199 (Gibco) containing 10% FBS. HT-29 cells were
379 cultured in complete DMEM/F12 (Thermo-Fisher) supplemented with sodium pyruvate, non-
380 essential amino acids, and HEPES. Vero E6-TMPRSS2 cells were generated using a lentivirus
381 vector. Briefly, HEK293T producer cells were transfected with pLX304-TMPRSS2, pCAGGS-
382 VSV-G, and psPAX2, and cell culture supernatants were collected at 48 hours and clarified by
383 centrifugation at 1,000 x g for 5 min. The resulting lentivirus was used to infect Vero E6 cells for
384 24 h, and cells were selected with 40 µg/ml blasticidin for 7 days.

385 **Recombinant VSV.** Recovery of recombinant VSV was performed as described (Whelan
386 et al., 1995). Briefly, BSRT7/5 cells were inoculated with vaccinia virus vTF7-3 and subsequently
387 transfected with T7-expression plasmids encoding VSV N, P, L, and G, and an antigenomic copy
388 of the viral genome. Cell culture supernatants were collected at 56-72 h, clarified by centrifugation
389 (5 min at 1,000 x g), and filtered through a 0.22 µm filter. Virus was plaque-purified on Vero CCL81
390 cells in the presence of 25 µg/ml of cytosine arabinoside (TriLink BioTechnologies), and plaques
391 in agarose plugs were amplified on Vero CCL81 cells. Viral stocks were amplified on MA104 cells

392 at an MOI of 0.01 in Medium 199 containing 2% FBS and 20 mM HEPES pH 7.7 (Millipore Sigma)
393 at 34°C. Viral supernatants were harvested upon extensive cytopathic effect and clarified of cell
394 debris by centrifugation at 1,000 x g for 5 min. Aliquots were maintained at -80°C.

395 **Next generation sequencing.** Total RNA was extracted from Vero CCL81 cells infected
396 with VSV-SARS-CoV-2-S_{Δ21} using Trizol (Invitrogen) according to the manufacturer's protocol.
397 RNA was used to generate next generation sequencing libraries using TruSeq Stranded Total
398 RNA library kit with Ribo Zero ribosomal subtraction (Illumina). The libraries were quantified using
399 a bioanalyzer (Agilent) and pooled at an equal molar concentration and used to generate paired
400 end 250 bp reads on an MiSeq (Illumina). Raw sequencing data was processed using fastp
401 v0.20.0 to trim adapters and filter out reads with a quality score < 30. Alignment of each sample
402 to VSV and SARS CoV-2 sequence was performed using bbmap v38.79. Mapped reads were
403 extracted using samtools 1.9 and used for de novo assembly by SPAdes v3.13.0. Consensus
404 sequences for each RNA sample were generated by aligning contigs to the reference plasmid
405 sequence pVSV(1+)-eGFP-SARS-CoV-2-S with SnapGene v5.0.

406 **Western blotting.** Purified VSV were incubated in non-reducing denaturation buffer (55
407 mM Tris-HCl pH 6.8, 1.67 % (w/v) SDS, 7.5 % (w/v) glycerol) at 100°C for 5 min. Viral proteins
408 were separated on a 8% acrylamide gel, transferred onto a nitrocellulose membrane, and
409 incubated with human anti-SARS antibody CR3022 diluted in Tris-buffer saline containing 1%
410 Tween-20 (TBS-T) and 5% milk, followed by incubation with HRP-conjugated goat anti-human
411 antibody (Abcam) diluted in TBS-T containing 1% milk. HRP activity was visualized using the
412 Pierce ECL Western blotting kit (Thermo Scientific) and imaged with a ChemiDoc™ MP Imager
413 (Bio-Rad).

414 **Metabolic radiolabeling of virions.** To generate high titer stocks of VSV-SARS-CoV-2,
415 BSRT7/5 cells were transfected with pCAGGS-VSV-G in Opti-MEM (Gibco) using Lipofectamine
416 2000 (Invitrogen) and infected 7 h later with VSV-SARS-CoV-2-S_{Δ21} at an MOI of 0.1 in DMEM
417 containing 2% FBS and 20 mM HEPES pH 7.7. Viral stocks were collected at 48 hpi, and used to

418 infect fresh cells (MOI of 10) for labeling of viral proteins. At 4 hpi, cells were starved in serum
419 free, methionine/cysteine free DMEM (Corning), and exposed to 15 μ Ci/ml [35 S]-methionine and
420 [35 S]-cysteine (Perkin Elmer) from 5-24 hours. Cell culture supernatants were collected, clarified
421 by centrifugation (1,500 x g, 5 min), and analyzed by SDS-PAGE and detected by phosphoimage
422 analysis (Li et al., 2006).

423 **Transmission electron microscopy.** Purified viruses were adhered to glow-discharged,
424 carbon-coated copper grids. Samples were stained with 2% (w/v) phosphotungstic acid, pH 7.1,
425 in H₂O and viewed on a JEOL 1200 EX transmission electron microscope (JEOL USA Inc.)
426 equipped with an AMT 8-megapixel digital camera and AMT Image Capture Engine V602
427 software (Advanced Microscopy Techniques).

428 **Monoclonal antibodies.** Phage-displayed Fab libraries were panned against immobilized
429 SARS-CoV-2 spike RBD in multiple rounds using established methods (Persson et al., 2013).
430 Following four rounds of selection, phage ELISAs were used to screen 384 clones to identify
431 those that bound specifically to RBD. The complementarity determining regions of Fab-phage
432 clones were decoded by sequencing the variable regions and cloning them into mammalian
433 expression vectors for expression and purification of human IgG1 proteins, as described (Tao et
434 al., 2019). A subset of the panel of mAbs was tested for neutralization as a part of this study.

435 Another set of mAbs (S304, S306, S309, S310 and S315) were isolated from EBV-
436 immortalized memory B cells from a SARS-CoV survivor (Traggiai et al., 2004) and are cross-
437 reactive to SARS-CoV-2 (Pinto et al, in press). Recombinant antibodies were expressed in
438 ExpiCHO cells transiently co-transfected with plasmids expressing the heavy and light chain as
439 previously described (Stettler et al., 2016).

440 **Human sera.** Human samples were collected from PCR-confirmed COVID-19 patients.
441 Serum samples were obtained by routine phlebotomy at different days post symptom onset
442 (range: day 5 - 20). Samples were prescreened by the Euroimmun anti-SARS-CoV-2 IgG ELISA
443 (Lubeck, Germany), a qualitative assay with the Food and Drug Administration Emergency Use

444 Authorization that detects antibodies to the SARS-CoV-2 S protein. This study was approved by
445 the Mayo Clinic Institutional Review Board.

446 **Protein expression and purification.** DNA fragments encoding human ACE2 (hACE2
447 residues 1-615) and mouse ACE2 (mACE2, residues 1-615) were synthesized and cloned into
448 pFM1.2 with a C-terminal HRV-3C protease cleavage site (LEVLFQGP) and a human IgG1 Fc
449 region as previously described (Raj et al., 2013). We transiently transfected plasmids into
450 Expi293F cells and harvested cell supernatants 4 days post transfection. Secreted hACE2-Fc and
451 mACE2-Fc proteins were purified by protein A chromatography (Goldbio).

452 **GFP-reduction neutralization test.** Patient samples were heat-inactivated at 56°C for 30
453 min. Indicated dilutions of samples were incubated with 10^2 PFU of VSV-SARS-CoV-2-S $_{\Delta 21}$ for 1
454 h at 37°C. Antibody-virus complexes were added to Vero E6 cells in 96-well plates and incubated
455 at 37°C for 7.5 h. Cells subsequently were fixed in 2% formaldehyde containing 10 µg/mL Hoechst
456 33342 nuclear stain (Invitrogen) for 45 min at room temperature, when fixative was replaced with
457 PBS. Images were acquired with the InCell 2000 Analyzer (GE Healthcare) automated
458 microscope in both the DAPI and FITC channels to visualize nuclei and infected cells (*i.e.*, eGFP-
459 positive cells), respectively (4X objective, 4 fields per well, covering the entire well). Images were
460 analyzed using the Multi Target Analysis Module of the InCell Analyzer 1000 Workstation
461 Software (GE Healthcare). GFP-positive cells were identified in the FITC channel using the top-
462 hat segmentation method and subsequently counted within the InCell Workstation software. The
463 sensitivity and accuracy of GFP-positive cell number determinations were validated using a serial
464 dilution of virus. A background number of GFP+ cells was subtracted from each well using an
465 average value determined from at least 4 uninfected wells. Data were processed using Prism
466 software (GraphPad Prism 8.0). ACE2 neutralization assays using VSV-SARS-CoV-2-S $_{\Delta 21}$ were
467 conducted similarly but using an MOI of 1.

468 **Focus reduction neutralization test.** SARS-CoV-2 strain 2019 n-CoV/USA_WA1/2020
469 was obtained from the Centers for Disease Control and Prevention (gift of Natalie Thornburg).
470 Virus was passaged in the indicated producer cells. Indicated dilutions of mAbs, sera, or protein
471 were incubated with 10^2 FFU of SARS-CoV-2 for 1 h at 37°C. Antibody-virus complexes were
472 added to indicated cell monolayers in 96-well plates and incubated at 37°C for 1 h. Subsequently,
473 cells were overlaid with 1% (w/v) methylcellulose in MEM supplemented with 2% FBS. Plates
474 were harvested 30 h later by removing overlays and fixed with 4% paraformaldehyde in PBS for
475 20 min at room temperature. Plates were washed and sequentially incubated with 1 µg/mL of
476 CR3022 anti-S antibody (ter Meulen et al., 2006; Yuan et al., 2020) and HRP-conjugated goat
477 anti-human IgG in PBS supplemented with 0.1% saponin and 0.1% BSA. SARS-CoV-2-infected
478 cell foci were visualized using TrueBlue peroxidase substrate (KPL) and quantitated on an
479 ImmunoSpot microanalyzer (Cellular Technologies). Data were processed using Prism software
480 (GraphPad Prism 8.0).

481 **Statistical analyses.** All statistical tests were performed using GraphPad Prism 8.0
482 software as described in the indicated figure legends.

483
484
485
486
487
488
489
490
491
492
493
494
495
496
497
498
499
500
501
502
503
504
505
506
507
508
509
510
511
512
513
514
515
516
517
518
519
520
521
522
523
524
525
526
527
528
529
530
531

REFERENCES

- Bai, Y., Yao, L., Wei, T., Tian, F., Jin, D.Y., Chen, L., and Wang, M. (2020). Presumed Asymptomatic Carrier Transmission of COVID-19. *JAMA*.
- Bloch, E.M., Shoham, S., Casadevall, A., Sachais, B.S., Shaz, B., Winters, J.L., van Buskirk, C., Grossman, B.J., Joyner, M., Henderson, J.P., *et al.* (2020). Deployment of convalescent plasma for the prevention and treatment of COVID-19. *J Clin Invest*.
- Carette, J.E., Raaben, M., Wong, A.C., Herbert, A.S., Obernosterer, G., Mulherkar, N., Kuehne, A.I., Kranzusch, P.J., Griffin, A.M., Ruthel, G., *et al.* (2011). Ebola virus entry requires the cholesterol transporter Niemann-Pick C1. *Nature* **477**, 340-343.
- Chen, J., Kovacs, J.M., Peng, H., Rits-Volloch, S., Lu, J., Park, D., Zablowsky, E., Seaman, M.S., and Chen, B. (2015). HIV-1 ENVELOPE. Effect of the cytoplasmic domain on antigenic characteristics of HIV-1 envelope glycoprotein. *Science* **349**, 191-195.
- Chen, L., Xiong, J., Bao, L., and Shi, Y. (2020). Convalescent plasma as a potential therapy for COVID-19. *Lancet Infect Dis* **20**, 398-400.
- Denison, M.R., Graham, R.L., Donaldson, E.F., Eckerle, L.D., and Baric, R.S. (2011). Coronaviruses: an RNA proofreading machine regulates replication fidelity and diversity. *RNA biology* **8**, 270-279.
- Fukushi, S., Mizutani, T., Saijo, M., Kurane, I., Taguchi, F., Tashiro, M., and Morikawa, S. (2006). Evaluation of a novel vesicular stomatitis virus pseudotype-based assay for detection of neutralizing antibody responses to SARS-CoV. *J Med Virol* **78**, 1509-1512.
- Fukushi, S., Mizutani, T., Saijo, M., Matsuyama, S., Miyajima, N., Taguchi, F., Itamura, S., Kurane, I., and Morikawa, S. (2005). Vesicular stomatitis virus pseudotyped with severe acute respiratory syndrome coronavirus spike protein. *J Gen Virol* **86**, 2269-2274.
- Garbutt, M., Liebscher, R., Wahl-Jensen, V., Jones, S., Moller, P., Wagner, R., Volchkov, V., Klenk, H.D., Feldmann, H., and Stroher, U. (2004). Properties of replication-competent vesicular stomatitis virus vectors expressing glycoproteins of filoviruses and arenaviruses. *J Virol* **78**, 5458-5465.
- Giroglou, T., Cinatl, J., Jr., Rabenau, H., Drosten, C., Schwalbe, H., Doerr, H.W., and von Laer, D. (2004). Retroviral vectors pseudotyped with severe acute respiratory syndrome coronavirus S protein. *J Virol* **78**, 9007-9015.
- Guan, W.J., Ni, Z.Y., Hu, Y., Liang, W.H., Ou, C.Q., He, J.X., Liu, L., Shan, H., Lei, C.L., Hui, D.S.C., *et al.* (2020). Clinical Characteristics of Coronavirus Disease 2019 in China. *N Engl J Med* **382**, 1708-1720.
- Hoffmann, M., Kleine-Weber, H., Schroeder, S., Kruger, N., Herrler, T., Erichsen, S., Schiergens, T.S., Herrler, G., Wu, N.H., Nitsche, A., *et al.* (2020). SARS-CoV-2 Cell Entry Depends on ACE2 and TMPRSS2 and Is Blocked by a Clinically Proven Protease Inhibitor. *Cell* **181**, 271-280.

532 Jae, L.T., Raaben, M., Herbert, A.S., Kuehne, A.I., Wirchnianski, A.S., Soh, T.K., Stubbs, S.H.,
533 Janssen, H., Damme, M., Saftig, P., *et al.* (2014). Virus entry. Lassa virus entry requires a trigger-
534 induced receptor switch. *Science* 344, 1506-1510.
535
536 Kobinger, G.P., Limberis, M.P., Somanathan, S., Schumer, G., Bell, P., and Wilson, J.M. (2007).
537 Human immunodeficiency viral vector pseudotyped with the spike envelope of severe acute
538 respiratory syndrome coronavirus transduces human airway epithelial cells and dendritic cells.
539 *Hum Gene Ther* 18, 413-422.
540
541 Kruse, R.L. (2020). Therapeutic strategies in an outbreak scenario to treat the novel coronavirus
542 originating in Wuhan, China. *F1000Research* 9, 72.
543
544 Lei, C., Qian, K., Li, T., Zhang, S., Fu, W., Ding, M., and Hu, S. (2020). Neutralization of SARS-
545 CoV-2 spike pseudotyped virus by recombinant ACE2-Ig. *Nat Commun* 11, 2070.
546
547 Letko, M., Marzi, A., and Munster, V. (2020). Functional assessment of cell entry and receptor
548 usage for SARS-CoV-2 and other lineage B betacoronaviruses. *Nature microbiology* 5, 562-569.
549
550 Li, F., Li, W., Farzan, M., and Harrison, S.C. (2005). Structure of SARS coronavirus spike
551 receptor-binding domain complexed with receptor. *Science* 309, 1864-1868.
552
553 Li, J., Wang, J.T., and Whelan, S.P. (2006). A unique strategy for mRNA cap methylation used
554 by vesicular stomatitis virus. *Proc Natl Acad Sci U S A* 103, 8493-8498.
555
556 Li, W., Moore, M.J., Vasilieva, N., Sui, J., Wong, S.K., Berne, M.A., Somasundaran, M., Sullivan,
557 J.L., Luzuriaga, K., Greenough, T.C., *et al.* (2003). Angiotensin-converting enzyme 2 is a
558 functional receptor for the SARS coronavirus. *Nature* 426, 450-454.
559
560 Lontok, E., Corse, E., and Machamer, C.E. (2004). Intracellular targeting signals contribute to
561 localization of coronavirus spike proteins near the virus assembly site. *J Virol* 78, 5913-5922.
562
563 McBride, C.E., Li, J., and Machamer, C.E. (2007). The cytoplasmic tail of the severe acute
564 respiratory syndrome coronavirus spike protein contains a novel endoplasmic reticulum retrieval
565 signal that binds COPI and promotes interaction with membrane protein. *J Virol* 81, 2418-2428.
566
567 Moore, M.J., Dorfman, T., Li, W., Wong, S.K., Li, Y., Kuhn, J.H., Coderre, J., Vasilieva, N., Han,
568 Z., Greenough, T.C., *et al.* (2004). Retroviruses pseudotyped with the severe acute respiratory
569 syndrome coronavirus spike protein efficiently infect cells expressing angiotensin-converting
570 enzyme 2. *J Virol* 78, 10628-10635.
571
572 Mukherjee, S., Sirohi, D., Dowd, K.A., Chen, Z., Diamond, M.S., Kuhn, R.J., and Pierson, T.C.
573 (2016). Enhancing dengue virus maturation using a stable furin over-expressing cell line. *Virology*
574 497, 33-40.
575
576 Ou, X., Liu, Y., Lei, X., Li, P., Mi, D., Ren, L., Guo, L., Guo, R., Chen, T., Hu, J., *et al.* (2020).
577 Characterization of spike glycoprotein of SARS-CoV-2 on virus entry and its immune cross-
578 reactivity with SARS-CoV. *Nat Commun* 11, 1620.
579
580 Persson, H., Ye, W., Wernimont, A., Adams, J.J., Koide, A., Koide, S., Lam, R., and Sidhu, S.S.
581 (2013). CDR-H3 diversity is not required for antigen recognition by synthetic antibodies. *J Mol*
582 *Biol* 425, 803-811.

583 Pinto, D. Young-Jun Park, Martina Beltramello, Alexandra C. Walls, M. Alejandra Tortorici, Siro
584 Bianchi, Stefano Jaconi, Katja Culap, Fabrizia Zatta, Anna De Marco, Alessia Peter, Barbara
585 Guarino, Roberto Spreafico, Elisabetta Cameroni, James Brett Case, Rita E. Chen, Colin
586 Havenar-Daughton, Gyorgy Snell, Amalio Telenti, Herbert W. Virgin, Antonio Lanzavecchia,
587 Michael S. Diamond, Katja Fink, David Veessler and Davide Corti (2020). Cross-neutralization of
588 SARS-CoV and SARS-CoV-2 by a human monoclonal 2 antibody. *Nature* (in press)
589
590 Raj, V.S., Mou, H., Smits, S.L., Dekkers, D.H., Muller, M.A., Dijkman, R., Muth, D., Demmers,
591 J.A., Zaki, A., Fouchier, R.A., *et al.* (2013). Dipeptidyl peptidase 4 is a functional receptor for the
592 emerging human coronavirus-EMC. *Nature* **495**, 251-254.
593
594 Ruch, T.R., and Machamer, C.E. (2012). The coronavirus E protein: assembly and beyond.
595 *Viruses* **4**, 363-382.
596
597 Shen, C., Wang, Z., Zhao, F., Yang, Y., Li, J., Yuan, J., Wang, F., Li, D., Yang, M., Xing, L., *et al.*
598 (2020). Treatment of 5 Critically Ill Patients With COVID-19 With Convalescent Plasma. *JAMA*.
599
600 Stanifer, M.L., Cureton, D.K., and Whelan, S.P. (2011). A recombinant vesicular stomatitis virus
601 bearing a lethal mutation in the glycoprotein gene uncovers a second site suppressor that restores
602 fusion. *J Virol* **85**, 8105-8115.
603
604 Stettler, K., Beltramello, M., Espinosa, D.A., Graham, V., Cassotta, A., Bianchi, S., Vanzetta, F.,
605 Minola, A., Jaconi, S., Mele, F., *et al.* (2016). Specificity, cross-reactivity, and function of
606 antibodies elicited by Zika virus infection. *Science* **353**, 823-826.
607
608 Tao, Y., Mis, M., Blazer, L., Ustav, M.J., Steinhart, Z., Chidiac, R., Kubarakos, E., O'Brien, S.,
609 Wang, X., Jarvik, N., *et al.* (2019). Tailored tetravalent antibodies potently and specifically activate
610 Wnt/Frizzled pathways in cells, organoids and mice. *Elife* **8**.
611
612 ter Meulen, J., van den Brink, E.N., Poon, L.L., Marissen, W.E., Leung, C.S., Cox, F., Cheung,
613 C.Y., Bakker, A.Q., Bogaards, J.A., van Deventer, E., *et al.* (2006). Human monoclonal antibody
614 combination against SARS coronavirus: synergy and coverage of escape mutants. *PLoS Med* **3**,
615 e237.
616
617 Tortorici, M.A., and Veessler, D. (2019). Structural insights into coronavirus entry. *Adv Virus Res*
618 **105**, 93-116.
619
620 Traggiai, E., Becker, S., Subbarao, K., Kolesnikova, L., Uematsu, Y., Gismondo, M.R., Murphy,
621 B.R., Rappuoli, R., and Lanzavecchia, A. (2004). An efficient method to make human monoclonal
622 antibodies from memory B cells: potent neutralization of SARS coronavirus. *Nat Med* **10**, 871-
623 875.
624
625 Walls, A.C., Park, Y.J., Tortorici, M.A., Wall, A., McGuire, A.T., and Veessler, D. (2020). Structure,
626 Function, and Antigenicity of the SARS-CoV-2 Spike Glycoprotein. *Cell*.
627
628 Watanabe, Y., Allen, J.D., Wrapp, D., McLellan, J.S., and Crispin, M. (2020). Site-specific glycan
629 analysis of the SARS-CoV-2 spike. *Science*.
630
631 Whelan, S.P., Ball, L.A., Barr, J.N., and Wertz, G.T. (1995). Efficient recovery of infectious
632 vesicular stomatitis virus entirely from cDNA clones. *Proc Natl Acad Sci U S A* **92**, 8388-8392.

633 Wrapp, D., Wang, N., Corbett, K.S., Goldsmith, J.A., Hsieh, C.L., Abiona, O., Graham, B.S., and
634 McLellan, J.S. (2020). Cryo-EM structure of the 2019-nCoV spike in the prefusion conformation.
635 Science.

636

637 Yuan, M., Wu, N.C., Zhu, X., Lee, C.D., So, R.T.Y., Lv, H., Mok, C.K.P., and Wilson, I.A. (2020).
638 A highly conserved cryptic epitope in the receptor-binding domains of SARS-CoV-2 and SARS-
639 CoV. Science.

640

641 Zang, R., Gomez Castro, M., McCune, B.T., Zeng, Q., Rothlauf, P.W., Sonnek, N.M., Liu, Z.,
642 Brulois, K.F., Wang, X., Greenberg, H.B., *et al.* (2020). TMPRSS2 and TMPRSS4 promote SARS-
643 CoV-2 infection of human small intestinal enterocytes. Science Immunology, In press.

644

645 Zhang, T., Wu, Q., and Zhang, Z. (2020). Probable Pangolin Origin of SARS-CoV-2 Associated
646 with the COVID-19 Outbreak. Curr Biol.

647

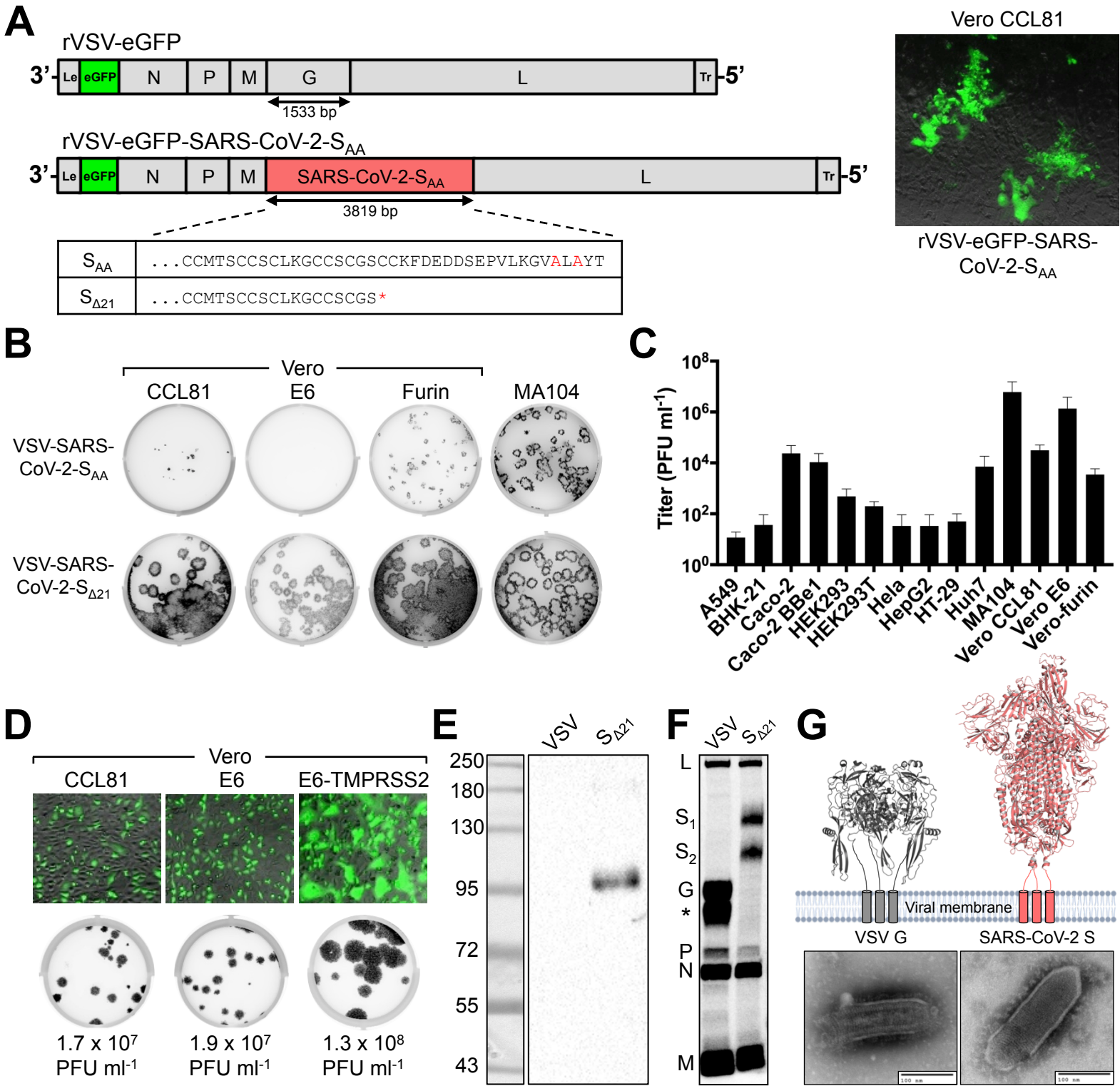
648 Zhou, P., Yang, X.L., Wang, X.G., Hu, B., Zhang, L., Zhang, W., Si, H.R., Zhu, Y., Li, B., Huang,
649 C.L., *et al.* (2020). A pneumonia outbreak associated with a new coronavirus of probable bat
650 origin. Nature 579, 270-273.

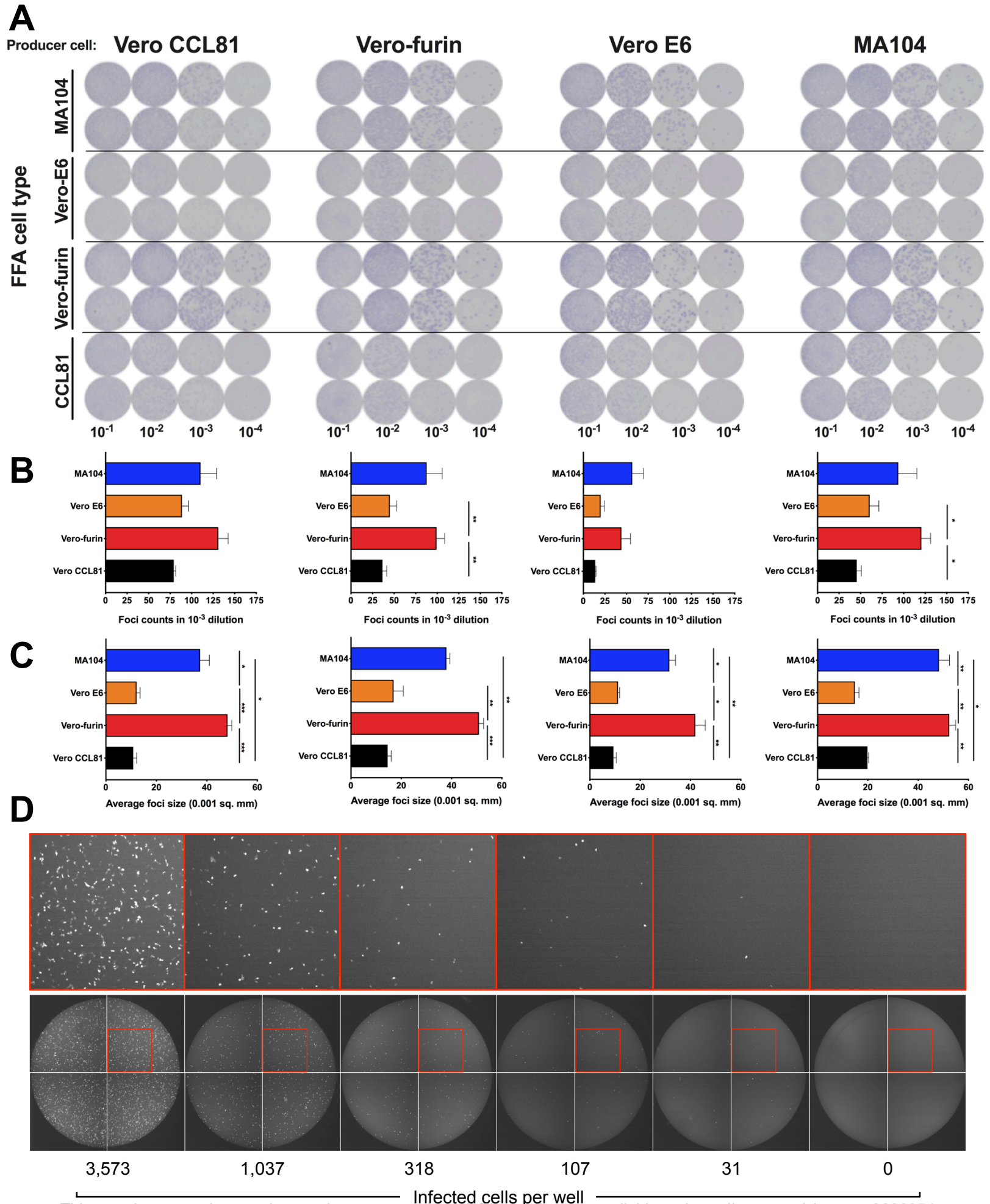
651

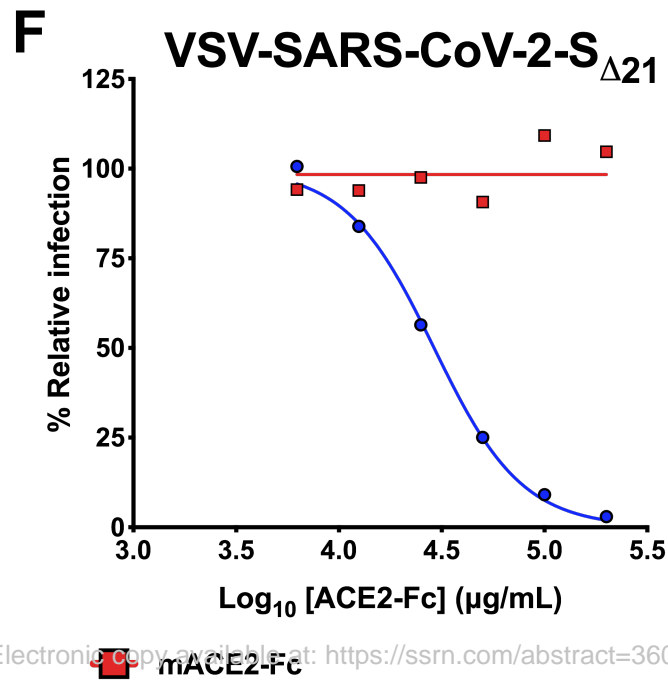
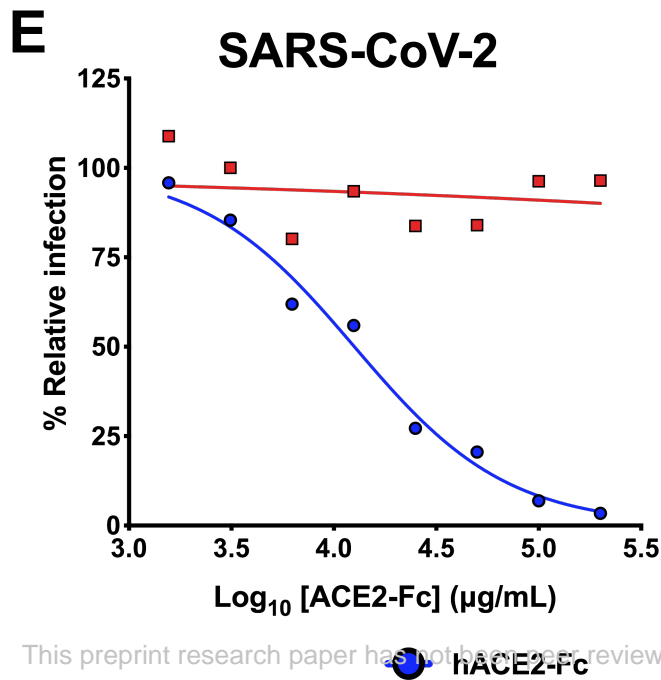
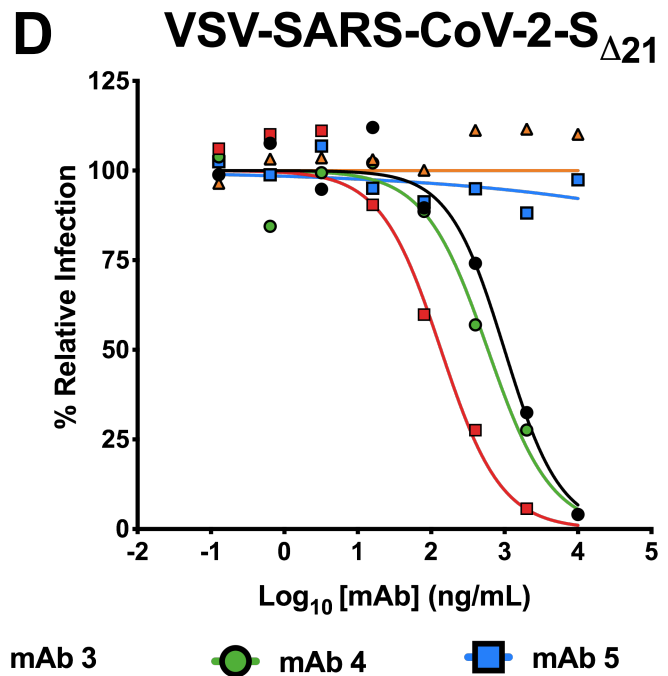
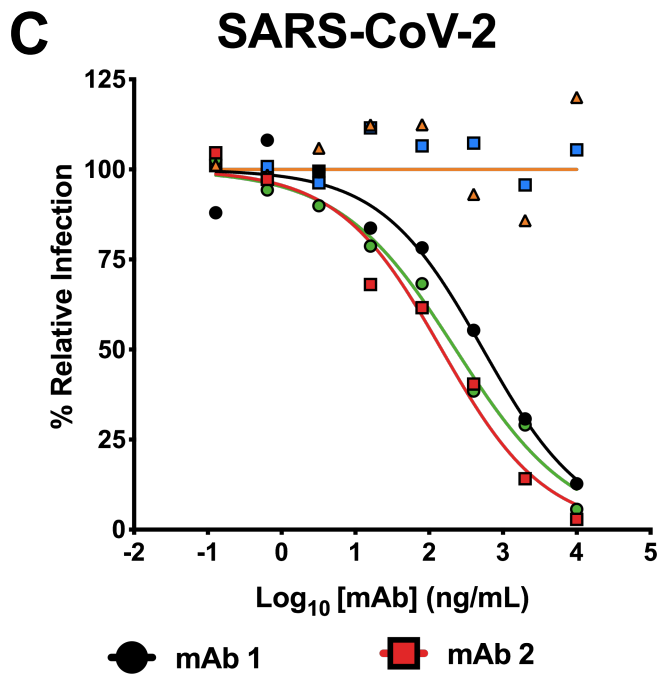
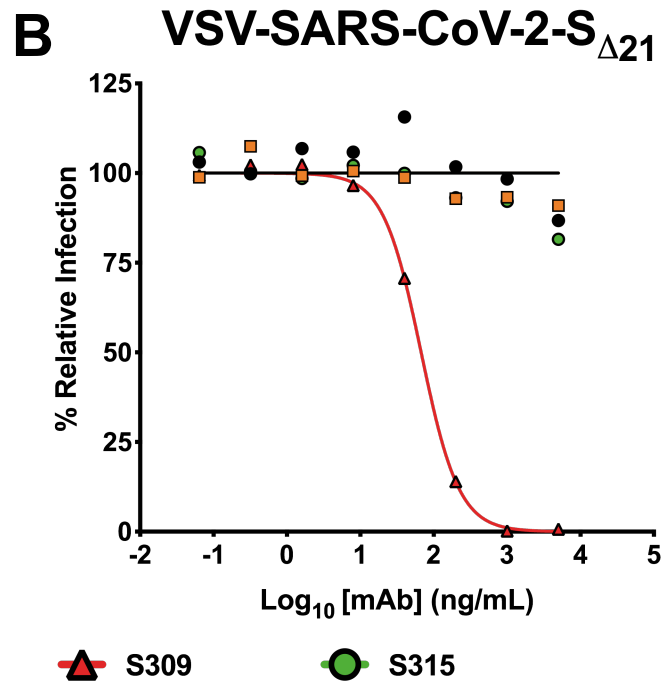
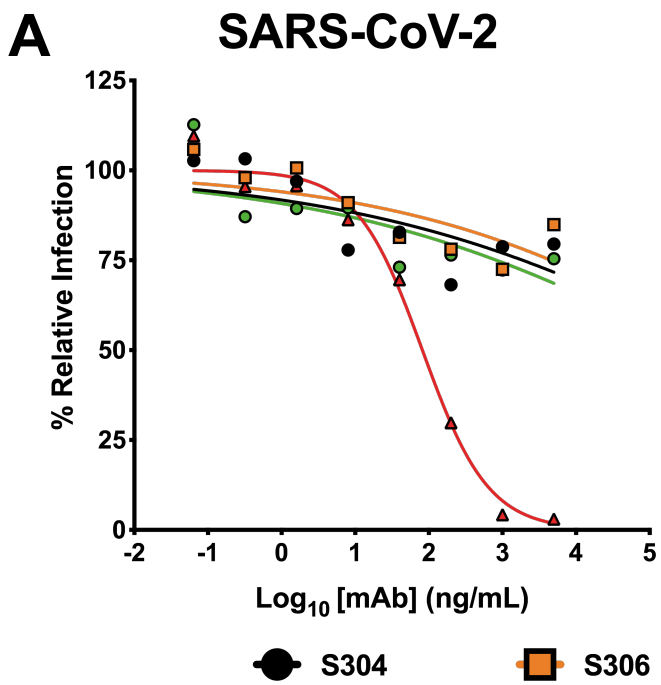
Table 1. Human serum ELISA IgG.

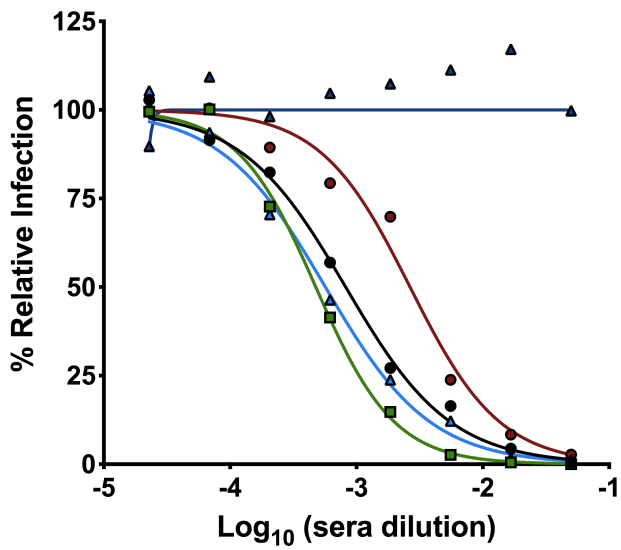
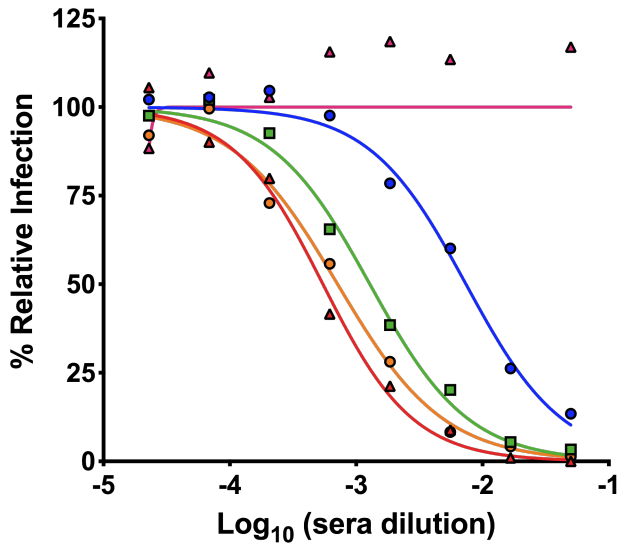
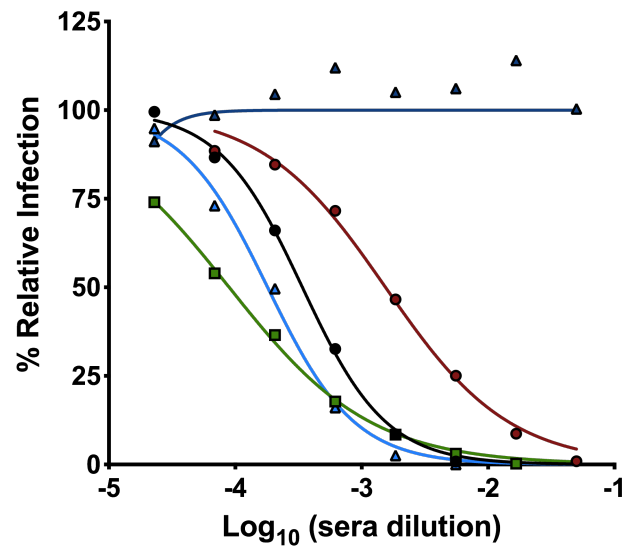
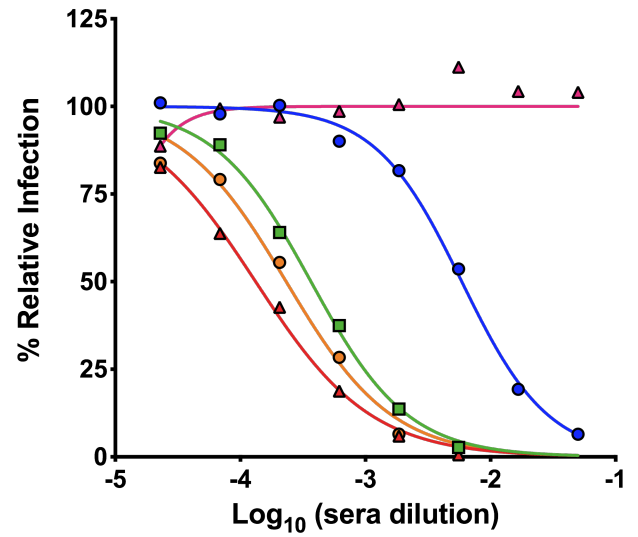
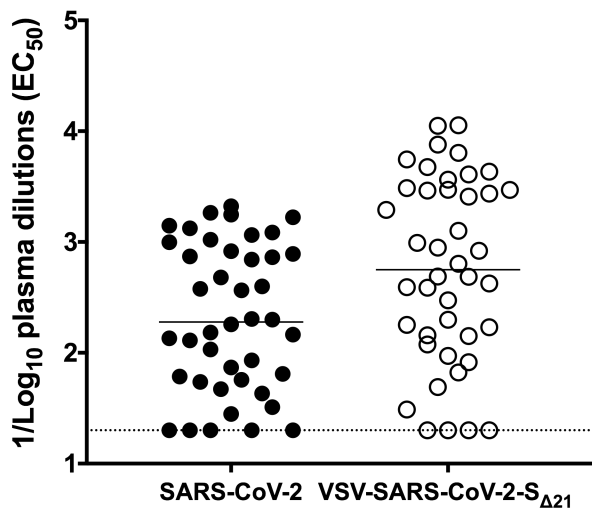
Serum	Days post symptom onset	Euroimmun IgG		Epitope IgG	
		Index	Reactive	Index	Reactive
1	14	1.3	+	2.6	+
2	12	6.0	+	3.5	+
3	17	10.2	+	3.9	+
4	16	14.9	+	4.5	+
5	5	0.2	-	1.2	+
6	19	8.6	+	4.4	+
7	17	7.1	+	4.1	+
8	10	5.1	+	2.0	+
9	14	6.8	+	3.1	+
10	6	0.2	-	1.1	+
11	-	5.6	+	0.9	+/-
12	-	<0.8	-	1.3	+
13	9	0.7	-	1.1	+
14	20	3.6	+	2.9	+
15	13	0.4	-	2.0	+
16	13	0.5	-	0.9	-
17	11	0.3	-	0.8	-
18	10	0.2	-	0.7	-
19	14	0.9	+/-	1.2	+
20	10	0.4	-	1.5	+
21	11	0.5	-	2.0	+
22	10	0.3	-	0.6	-
23	17	7.6	+	4.2	+
24	14	3.5	+	3.3	+
25	13	1.5	+	2.9	+
26	17	14.2	+	4.4	+
27	13	0.5	-	1.9	+
28	14	9.2	+	4.6	+
29	13	3.9	+	2.8	+
30	16	3.4	+	4.6	+
31	15	10.7	+	3.6	+
32	6	0.5	-	1.1	+
33	11	0.4	-	1.8	+
34	12	0.6	-	2.5	+
35	14	3.7	+	4.1	+
36	20	11.6	+	4.2	+
37	7	0.7	-	1.2	+
38	8	1.7	+	1.9	+
39	7	0.3	-	0.7	-
40	9	3.4	+	2.2	+
41	18	10.3	+	4.1	+
42	17	10.3	+	4.6	+

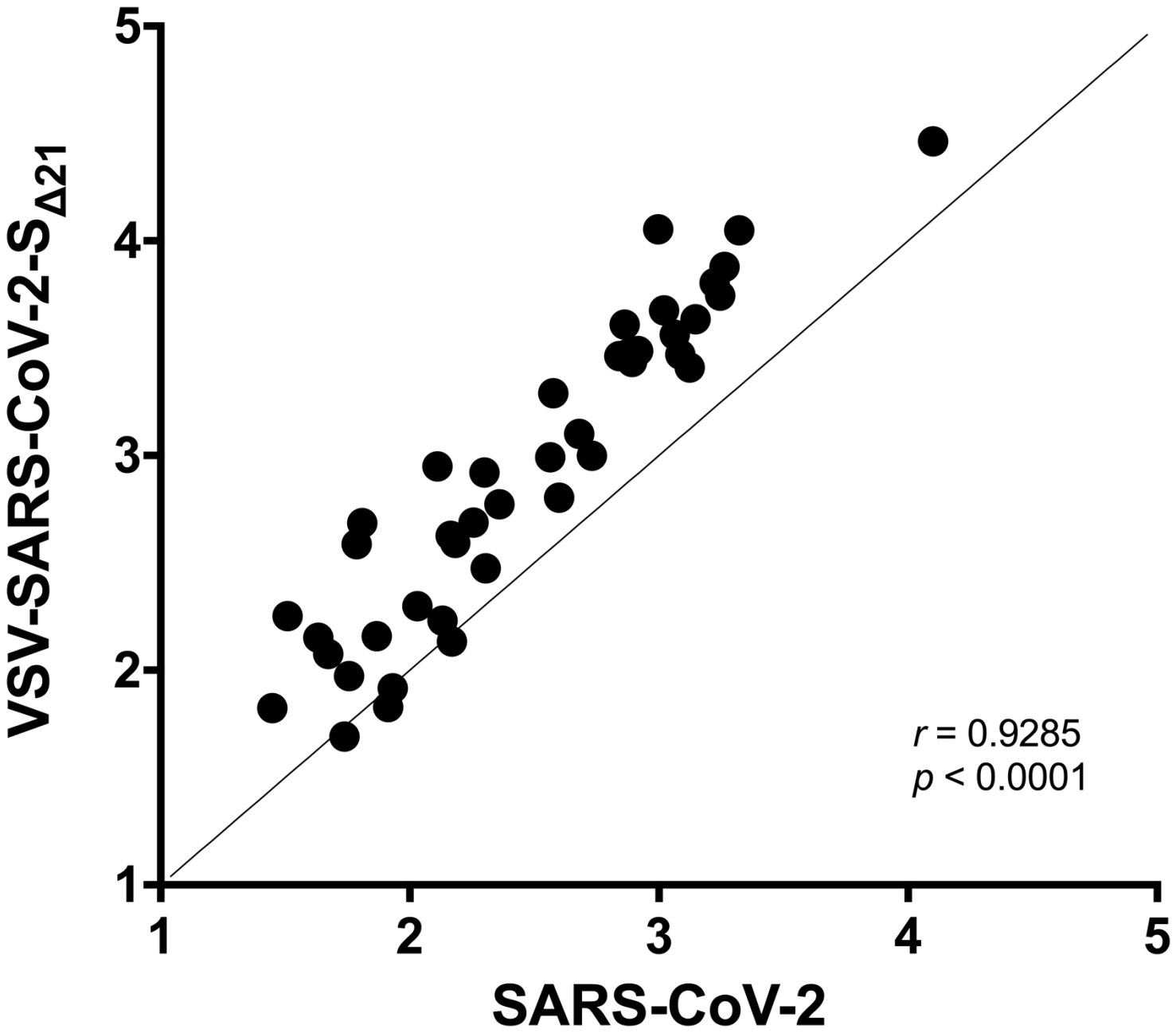
Legend to Table 1: Serum samples from 20 individuals were collected at different time points post onset of COVID-19 symptoms, were screened using two ELISA assays (Euroimmun or Epitope). The serum numbers correspond to those of Figures 4 and S3. IgG index values were calculated by dividing the O.D. of the serum sample by a reference O.D. control, and ratios were interpreted using the following criteria as recommended by the manufacturer: Negative (-) <0.8, Indeterminate (+/-) 0.8-1.1, Positive (+) ≥ 1.1 .



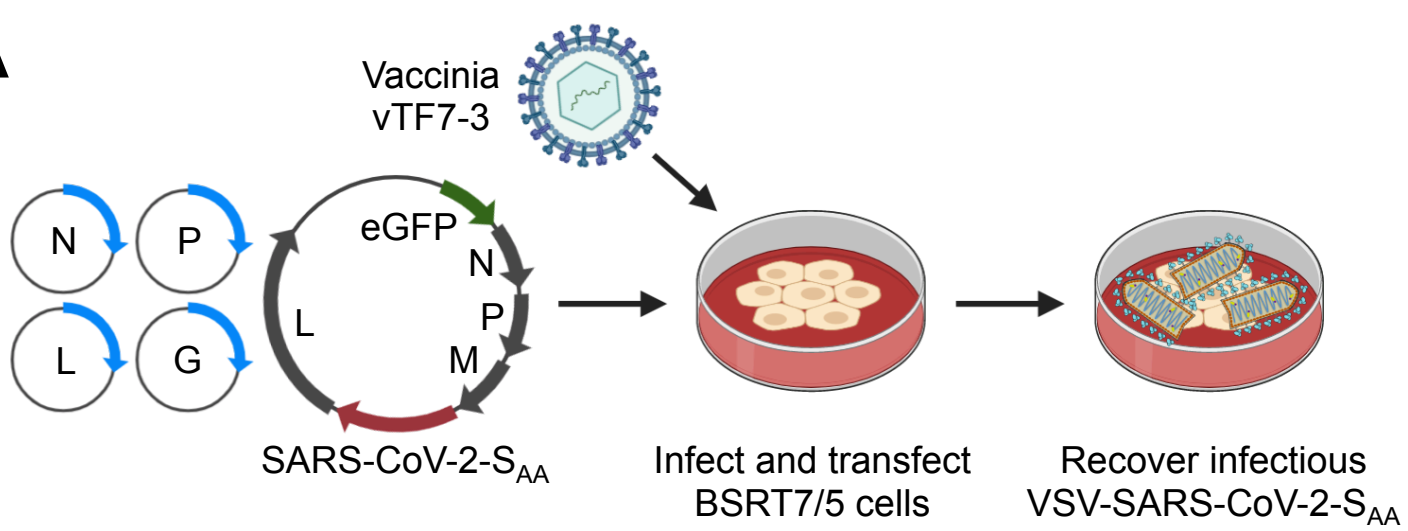




A SARS-CoV-2**B VSV-SARS-CoV-2-S_{Δ21}** Fig 4**C**



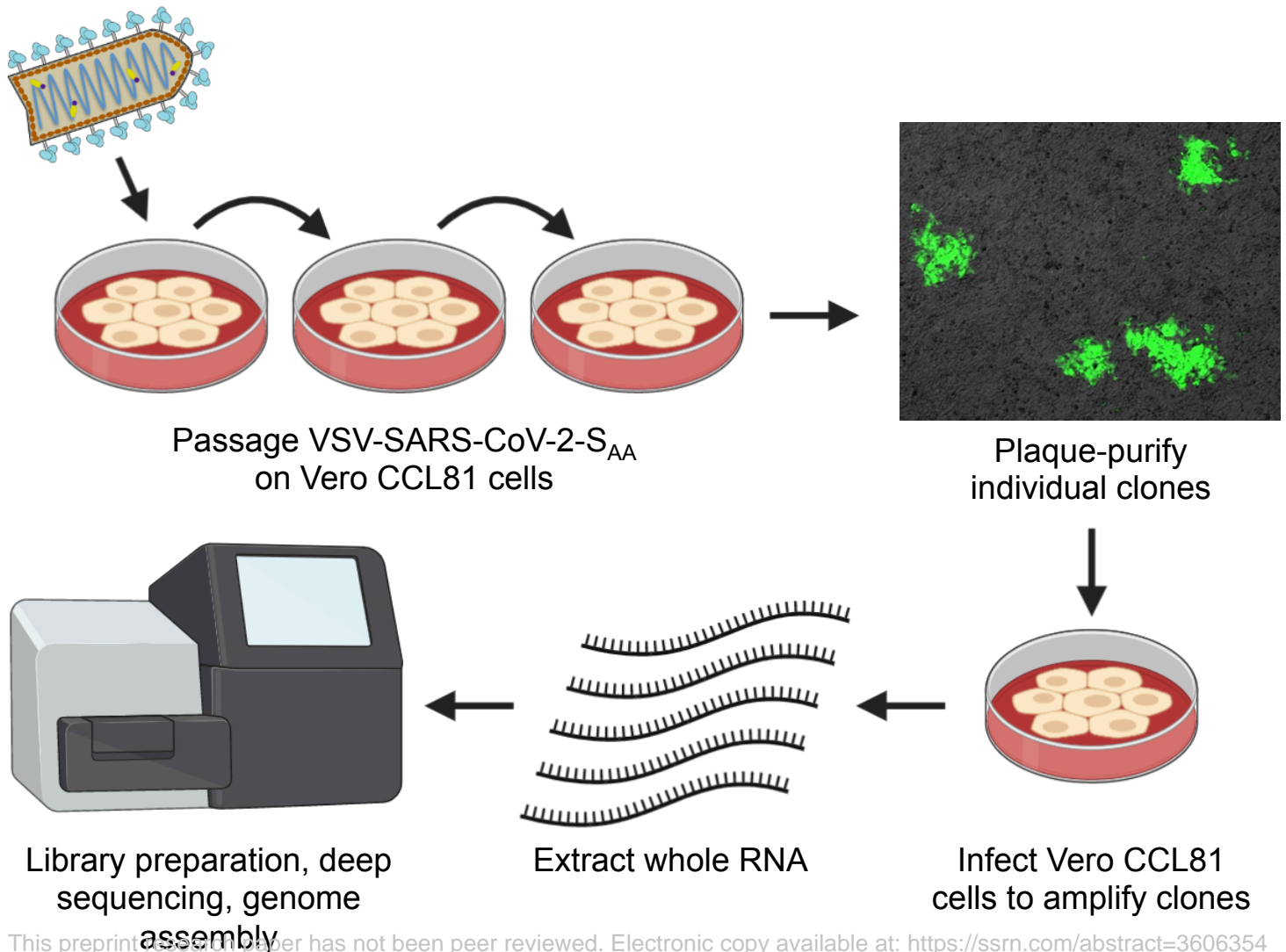
A

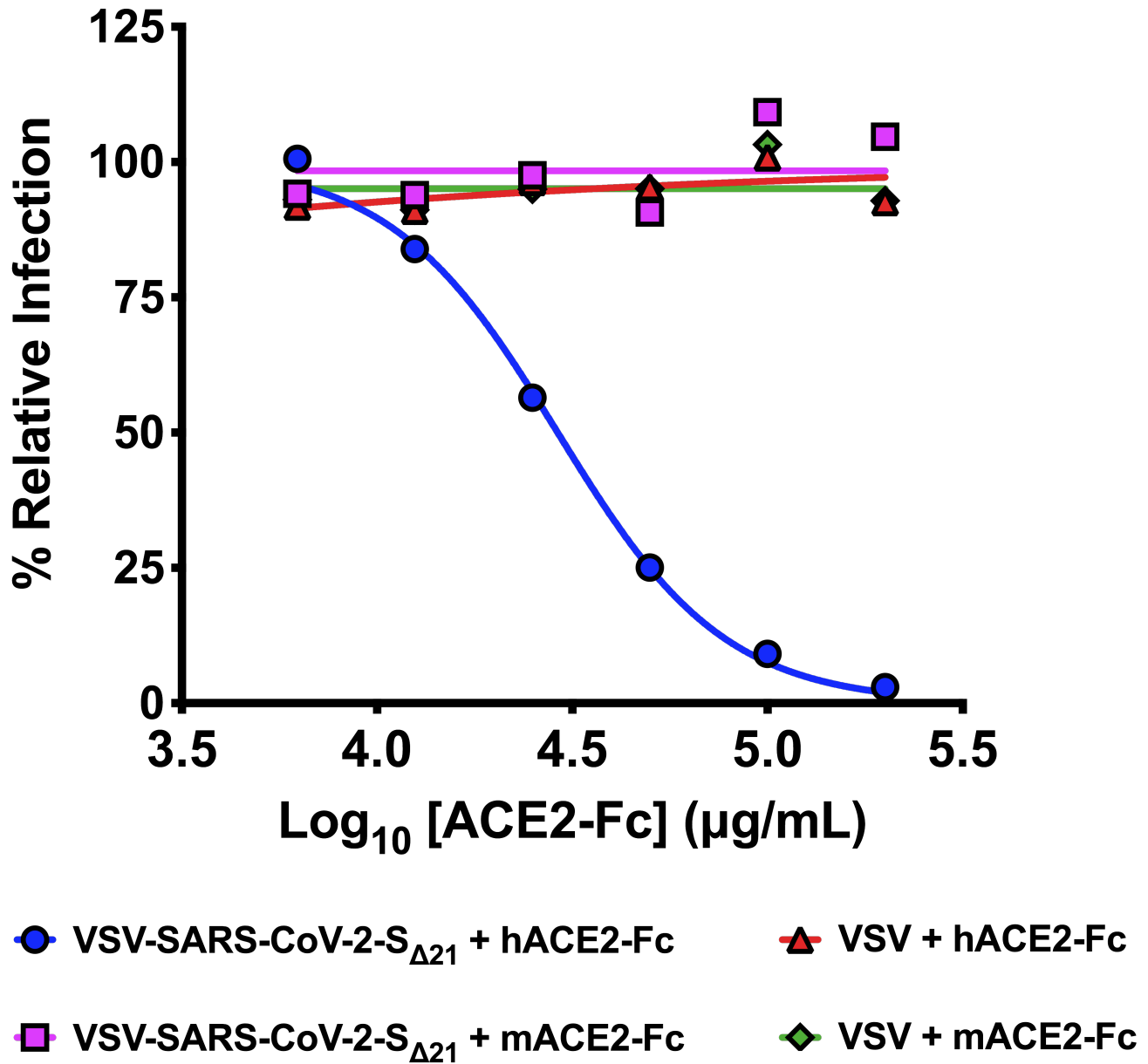


B

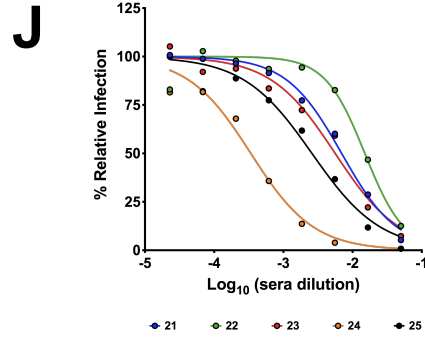
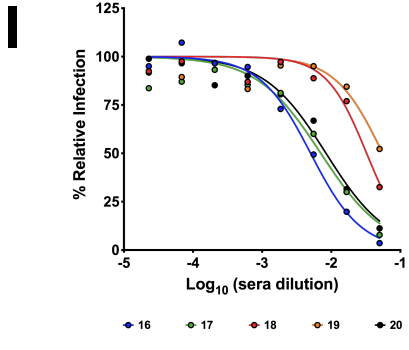
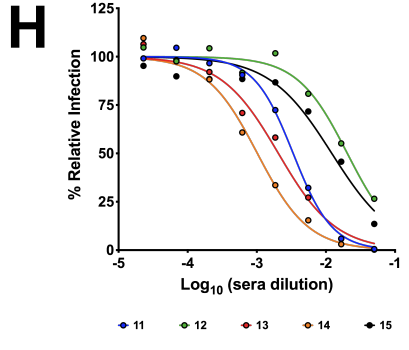
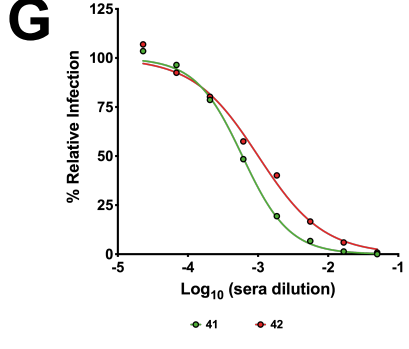
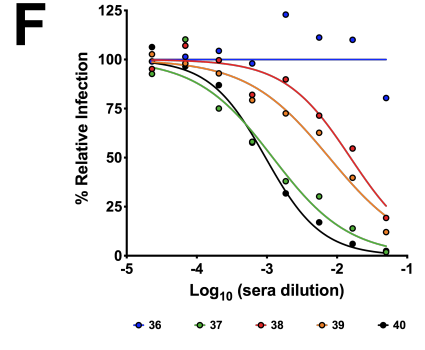
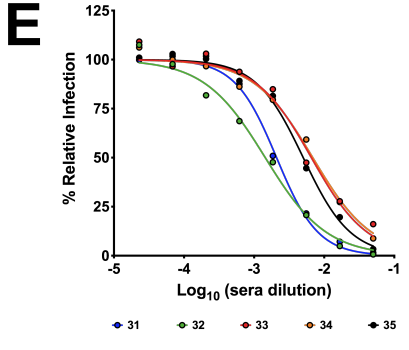
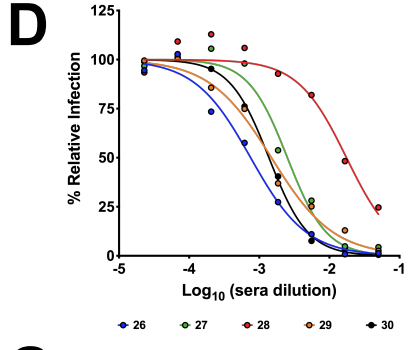
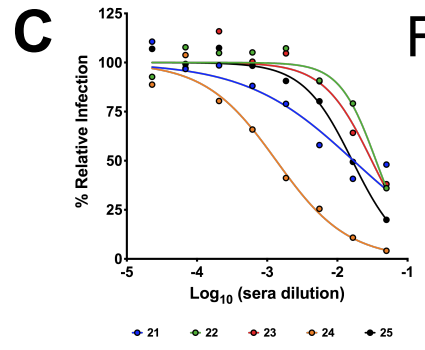
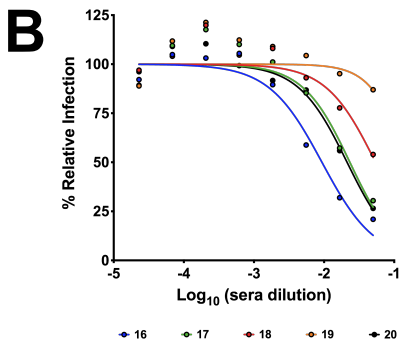
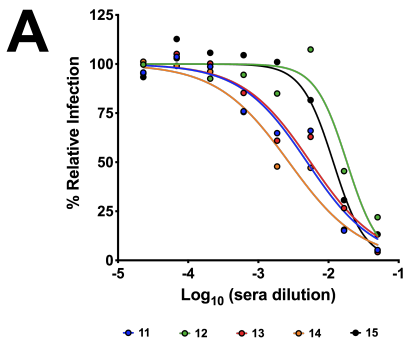
Tail Mutant	Amino acid sequence (membrane proximal region, transmembrane domain, cytoplasmic tail)	Rescue	Spread
S _{AA}	LNESLIDLQELGKYEQYIKWPWYIWLGFIAGLIAIVMVTIMLCCMTSCCCLKGCSCGSCCKFDEDDSEPVLKGVALAYT	+	+
MERS S _{AA}	LNESLIDLQELGKYEQYIKWPWYIWLGFIAGLIAIVMVTIMLKLKCNRCDDRYEEDLEPHAVAVH	+	-
VSV G #1	LNESLIDLQELGKYEQYIKWPWYIWLGFIAGLIAIVMVTIMLCCMTSCCCLRVGIYLCIKLKHTKKRQIYTDIEMNRLGK	+	-
VSV G #2	LNESLIDLQELGKYEQYIKWPWYIWLGFIAGLIAIVMVTIMLRVGIYLCIKLKHTKKRQIYTDIEMNRLGK	+	-
VSV G TM/tail	LNESLIDLQELGKYEQYIKWSSIASFCFIIGLIIGLFLVLRVGIYLCIKLKHTKKRQIYTDIEMNRLGK	+	-
VSV G Ecto/TM/tail	LNEGWFSSWKSSIASFCFIIGLIIGLFLVLRVGIYLCIKLKHTKKRQIYTDIEMNRLGK	+	-

C

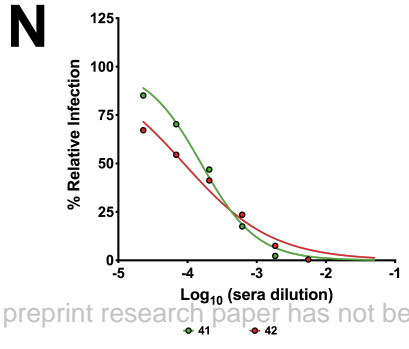
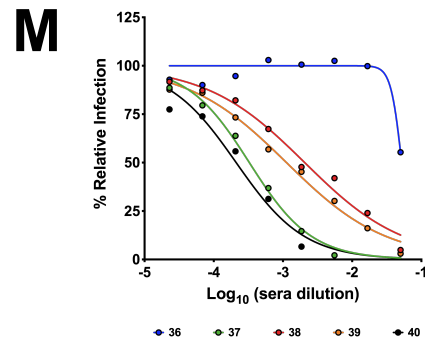
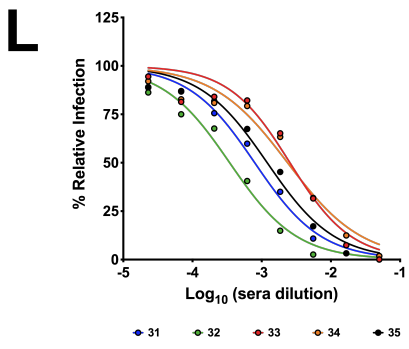
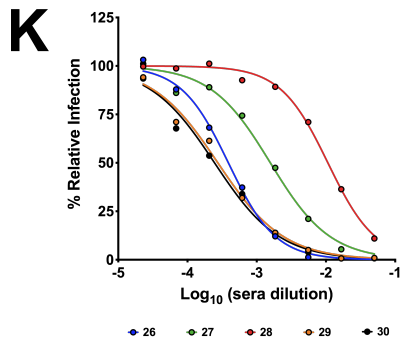




SARS-CoV-2



VSV-SARS-CoV-2-S_{Δ21}



Supplemental Data.

Antigenomic (+ sense) sequence of VSV-eGFP-SARS-CoV-2-S_{Δ21}:

5' ACGACAAACAAACCATTTATTATCATTTAAAAGGCTCAGGAGAAACTTTAACAGTAATCAGAAT
TCTCGAGATGGTGAGCAAGGGCGAGGAGCTGTTACCCGGGGTGGTGCCCATCCTGGTCGAGCTG
GACGGCGACGTAAACGGCCACAAGTTTCAGCGTGTCCGGCGAGGGCGAGGGCGATGCCACCTACG
GCAAGCTGACCCTGAAGTTCATCTGCACCACCGGCAAGCTGCCCGTGCCCTGGCCACCCTCGT
GACCACCCTGACCTACGGCGTGCAGTGCTTCAGCCGTACCCCGACCACATGAAGCAGCAGCAGC
TTCTTCAAGTCCGCCATGCCCGAAGGCTACGTCCAGGAGCGCACCATCTTCTTCAAGGACGACG
GCAACTACAAGACCCGCGCCGAGGTGAAGTTCGAGGGCGACACCCTGGTGAACCGCATCGAGCT
GAAGGGCATCGACTTCAAGGAGGACGGCAACATCCTGGGGCACAAGCTGGAGTACAACACTACAAC
AGCCACAACGTCTATATCATGGCCGACAAGCAGAAGAACGGCATCAAGGTGAACCTCAAGATCC
GCCACAACATCGAGGACGGCAGCGTGCAGCTCGCCGACCACTACCAGCAGAACACCCCCATCGG
CGACGGCCCCGTGCTGCTGCCCGACAACCACTACCTGAGCACCCAGTCCGCCCTGAGCAAAGAC
CCCAACGAGAAGCGCGATCACATGGTCTTGCTGGAGTTCGTGACCGCCGCCGGGATCACTCTCG
GCATGGACGAGCTGTACAAGTGATGGCCATATGAAAAAACTAACAGTAATCAAAATGTCTGTT
ACAGTCAAGAGAATCATTGACAACACAGTCATAGTTCCAAAACCTTCTGCAAATGAGGATCCAG
TGGAATACCCGGCAGATTACTTTCAGAAAATCAAAGGAGATTCTCTTTACATCAATACTACAAA
AAGTTTGTGATCTAAGAGGATATGTCTACCAAGGCCTCAAATCCGGAATGTATCAATCATA
CATGTCAACAGCTACTTGTATGGAGCATTAAGGACATCCGGGGTAAGTTGGATAAAGATTGGT
CAAGTTTCGGAATAAACATCGGGAAAGCAGGGGATACAATCGGAATATTTGACCTTGTATCCTT
GAAAGCCCTGGACGGCGTACTTCCAGATGGAGTATCGGATGCTTCCAGAACCAGCGCAGATGAC
AAATGGTTGCCTTTGTATCTACTTGGCTTATACAGAGTGGGCAGAACACAAATGCCTGAATACA
GAAAAAAGCTCATGGATGGGCTGACAAATCAATGCAAAATGATCAATGAACAGTTTGAACCTCT
TGTGCCAGAAGGTCGTGACATTTTTGATGTGTGGGGAAATGACAGTAATTACACAAAAAATTGTC
GCTGCAGTGGACATGTTCTTCCACATGTTCAAAAACATGAATGTGCCTCGTTCAGATACGGAA
CTATTGTTTCCAGATTCAAAGATTGTGCTGCATTTGGCAACATTTGGACACCTCTGCAAAAATAAC
CGGAATGTCTACAGAAGATGTAACGACCTGGATCTTGAACCGAGAAGTTGCAGATGAAATGGTC
CAAATGATGCTTCCAGGCCAAGAAATTGACAAGGCCGATTTCATACATGCCTTATTTGATCGACT
TTGGATTGTCTTCTAAGTCTCCATATTCTTCCGTCAAAAACCCTGCCTTCCACTTCTGGGGGCA
ATTGACAGCTCTTCTGCTCAGATCCACCAGAGCAAGGAATGCCCGACAGCCTGATGACATTGAG
TATACATCTCTTACTACAGCAGGTTTTGTTGTACGCTTATGCAGTAGGATCCTCTGCCGACTTGG
CACAACAGTTTTTGTGTTGGAGATAACAAATACACTCCAGATGATAGTACCGGAGGATTGACGAC
TAATGCACCGCCACAAGGCAGAGATGTGGTCGAATGGCTCGGATGGTTTGAAGATCAAAACAGA
AAACCGACTCCTGATATGATGCAGTATGCGAAAAGAGCAGTCATGTCACTGCAAGGCCTAAGAG
AGAAGACAATTGGCAAGTATGCTAAGTCAGAATTTGACAAATGACCCTATAATTTCTCAGATCAC
CTATTATATATTATGCTACATATGAAAAAACTAACAGATATCATGGATAATCTCACAAAAGTT
CGTGAGTATCTCAAGTCTACTCTCGTCTAGATCAGGCGGTAGGAGAGATAGATGAGATCGAAG
CACAACGAGCTGAAAAGTCCAATTATGAGTTGTTCCAAGAGGACGGAGTGGAAAGAGCATACTAG
GCCCTCTTATTTTCAGGCAGCAGATGATTCTGACACAGAATCTGAACCAGAAATTTGAAGACAAT
CAAGGCTTGTATGTACCAGATCCGGAAGCTGAGCAAGTTGAAGGCTTTATACAGGGGCCTTTAG
ATGACTATGCAGATGAGGACGTGGATGTTGTATTTCACTTCCGACTGGAAACAGCCTGAGCTTGA
ATCCGACGAGCATGGAAGACCTTACGGTTGACATTGCCAGAGGGTTTAAAGTGGAGAGCAGAAA
TCCCAGTGGCTTTTTCAGGATTAAGCAGTCGTTCAAAGTGCCAAACACTGGAATCTGGCAGAGT
GCACATTTGAAGCATCGGGAGAAGGGGTCATCATAAAAAAGCGCCAGATAACTCCGGATGTATA
TAAGGTCCTCCAGTGTGAACACACATCCGTACCAATCAGAAGCCGTATCAGATGTTTGGTCT
CTCTCAAAGACATCCATGACTTTCCAACCCAAGAAAGCAAGTCTTCAGCCTCTCACCATATCCT
TGGATGAATTGTTCTCATCTAGAGGAGAATTCATCTCTGTGCGAGGTAACGGACGAATGTCTCA

TAAAGAGGCCATCCTGCTCGGTCTGAGGTACAAAAAGTTGTACAATCAGGCGAGAGTCAAATAT
TCTCTGTAGACTATGAAAAAAGTAACAGATATCACAATCTAAGTGTTATCCCAATCCATTCAT
CATGAGTTCCTTAAAGAAGATTCTCGGTCTGAAGGGGAAAGGTAAGAAATCTAAGAAATTAGGG
ATCGCACCACCCCTTATGAAGAGGACACTAGCATGGAGTATGCTCCGAGCGCTCCAATTGACA
AATCCTATTTTGGAGTTGACGAGATGGACACCTATGATCCGAATCAATTAAGATATGAGAAAT
CTTCTTTACAGTGAAAAATGACGGTTAGATCTAATCGTCCGTTTCCAGAACATACTCAGATGTGGCA
GCCGCTGTATCCCATTTGGGATCACATGTACATCGGAATGGCAGGGAAACGTCCCTTCTACAAAA
TCTTGGCTTTTTTGGGTTCTTCTAATCTAAAGGCCACTCCAGCGGTATTGGCAGATCAAGGTCA
ACCAGAGTATCACGCTCACTGCGAAGGCAGGGCTTATTTGCCACATAGGATGGGGAAAGACCCCT
CCCATGCTCAATGTACCAGAGCACTTCAGAAGACCATTCAATATAGGTCTTTACAAGGGAACGA
TTGAGCTCACAATGACCATCTACGATGATGAGTCACTGGAAGCAGCTCCTATGATCTGGGATCA
TTTCAATTCTTCCAAATTTTCTGATTTTCCAGAGAGAAGGCCTTAATGTTTGGCCTGATTGTGCGAG
AAAAAGGCATCTGGAGCGTGGGTCCTGGATTCTATCAGCCACTTCAAATGAGCTAGTCTAGCTT
CCAGCTTCTGAACAATCCCCGGTTTACTCAGTCTCTCCTAATTCAGCCTTTTGAACAACCTAAT
ATCCTGTCTTTTTCTATCCCTATGAAAAAACTAACAGAGATCGATCTGTTTCCCTTGACACGCGT
ACCATGTTTGTTTTTCTTGTTTTTATTGCCACTAGTCTCTAGTCAGTGTGTTAATCTTACAACCA
GAACTCAATTACCCCTGCATACACTAATTTCTTTCACACGTGGTGTTTATTACCCTGACAAAGT
TTTCAGATCCTCAGTTTTACATTCAACTCAGGACTTGTTCTTACCTTTCTTTTCCAATGTTACT
TGGTTCCATGCTATAACATGTCTCTGGGACCAATGGTACTAAGAGGTTTGATAACCCCTGTCCTAC
CATTTAATGATGGTGTTTATTTTGGCTTCCACTGAGAAGTCTAACATAATAAGAGGCTGGATTTT
TGGTACTACTTTAGATTCGAAGACCCAGTCCCTACTTATTGTTAATAACGCTACTAATGTTGTT
ATTAAGTCTGTGAATTTCAATTTTGTAAATGATCCATTTTTGGGTGTTTATTACCACAAAAACA
ACAAAAGTTGGATGGAAAGTGAGTTCAGAGTTTATTCTAGTGCGAATAATTGCACTTTTGAATA
TGTCTCTCAGCCTTTTCTTATGGACCTTGAAGGAAAACAGGGTAATTTCAAAAATCTTAGGGAA
TTTGTGTTTAAAGAATATTGATGGTTATTTTAAAATATATTCTAAGCACACGCCTATTAATTTAG
TGCCTGATCTCCCTCAGGGTTTTTTCGGCTTTAGAACCATTGGTAGATTTGCCAATAGGTATTAA
CATCACTAGGTTTCAAACCTTTACTTGTCTTACATAGAAAGTTATTTGACTCCTGGTGATTCTTCT
TCAGGTTGGACAGCTGGTGTGCAGCTTATTATGTGGGTTATCTTCAACCTAGGACTTTTCTAT
TAAAATATAATGAAAATGGAACCATTACAGATGCTGTAGACTGTGCACTTGACCCTCTCTCAGA
AACAAAGTGTACGTTGAAATCCTTCACTGTAGAAAAAGGAATCTATCAAACCTTCTAACTTTAGA
GTCCAACCAACAGAATCTATTGTTAGATTTCCCTAATATTACAACTTGTGCCCTTTTGGTGAAG
TTTTTAACGCCACCAGATTTGCATCTGTTTATGCTTGGAAACAGGAAGAGAATCAGCAACTGTGT
TGCTGATTATTCTGTCTTATATAATTCCGCATCATTTTTCCACTTTTAAAGTGTATGGAGTGTCT
CCTACTAAATTAATGATCTCTGCTTTACTAATGTCTATGCAGATTCATTTGTAATTAGAGGTG
ATGAAGTCAGACAAATCGCTCCAGGGCAAACCTGGAAAGATTGCTGATTATAATTATAAATTACC
AGATGATTTTACAGGCTGCGTTATAGCTTGGAAATCTAACAACTTTGATTCTAAGGTTGGTGGT
AATTATAATTACCTGTATAGATTGTTTGGAAAGTCTAATCTCAAACCTTTTGGAGAGAGATATTT
CAACTGAAATCTATCAGGCCGGTAGCACACCTTGTAAATGGTGTGTAAGGTTTTAATTGTTACTT
TCCTTTACAATCATATGGTTTTCCAACCCACTAATGGTGTGGTTACCAACCATAACAGAGTAGTA
GTACTTTCTTTTGAACCTTCTACATGCACCAGCAACTGTTTGTGGACCTAAAAAGTCTACTAAT
TGGTTAAAAACAAATGTGTCAATTTCAACTTCAATGGTTTAAACAGGCACAGGTGTTCTTACTGA
GTCTAACAAAAAGTTTTCTGCCTTTCCAACAATTTGGCAGAGACATTGCTGACACTACTGATGCT
GTCCGTGATCCACAGACACTTGAGATTCTTGACATTACACCATGTTCTTTTGGTGGTGTGCTAGT
TTATAACACCAGGAACAAATACTTCTAACCAGGTTGCTGTTCTTTATCAGGATGTTAACTGCAC
AGAAGTCCCTGTTGCTATTTCATGCAGATCAACTTACTCCTACTTGGCGTGTTTATTCTACAGGT
TCTAATGTTTTTCAAACACGTGCAGGCTGTTTAAATAGGGGCTGAACATGTCAACAACCTCATATG
AGTGTGACATAACCATTGGTGCAGGTATATGCGCTAGTTATCAGACTCAGACTAATTTCTCCTCG

CGGGGCACGTAGTGTAGCTAGTCAATCCATCATTGCCTACACTATGTCACTTGGTGCAGAAAAT
TCAGTTGCTTACTCTAATAACTCTATTGCCATACCCACAAATTTTACTATTAGTGTACCACAG
AAATTCTACCAGTGTCTATGACCAAGACATCAGTAGATTGTACAATGTACATTTGTGGTGATTC
AACTGAATGCAGCAATCTTTTGTGCAATATGGCAGTTTTTGTACACAATTAACCGTGCTTTA
ACTGGAATAGCTGTTGAACAAGACAAAAACCCCAAGAAGTTTTTGCACAAGTCAAACAAATTT
ACAAAACACCACCAATTAAGATTTTTGGTGGTTTTAATTTTTTCACAAATATTACCAGATCCATC
AAAACCAAGCAAGAGGTCATTTATTGAAGATCTACTTTTTCAACAAAGTGACACTTGCAGATGCT
GGCTTCATCAAACAATATGGTGATTGCCTTGGTGATATTGCTGCTAGAGACCTCATTTGTGCAC
AAAAGTTTAACGGCCTTACTGTTTTGCCACCTTTGCTCACAGATGAAATGATTGCTCAATACAC
TTCTGCACTGTTAGCGGGTACAATCACTTCTGGTTGGACCTTTGGTGCAGGTGCTGCATTACAA
ATACCATTTGCTATGCAAATGGCTTATAGGTTTAATGGTATTGGAGTTACACAGAATGTTCTCT
ATGAGAACCAAAATTGATTGCCAACCAATTTAATAGTGCTATTGGCAAAATTCAGACTCACT
TTCTTCCACAGCAAGTGCCTTGGAAAACCTCAAGATGTGGTCAACCAAAATGCACAAGCTTTA
AACACGCTTGTAAACAACCTTAGCTCCAATTTTTGGTGCATTTCAAGTGTTTTAAATGATATCC
TTTCACGTCTTGACAAAGTTGAGGCTGAAGTGCAAATGATAGGTTGATCACAGGCAGACTTCA
AAGTTTGCAGACATATGTGACTCAACAATTAATTAGAGCTGCAGAAATCAGAGCTTCTGCTAAT
CTTGCTGCTACTAAAATGTCAGAGTGTGTACTTGGACAATCAAAAAGAGTTGATTTTTGTGGAA
AGGGCTATCATCTTATGTCCTTCCCTCAGTCAGCACCTCATGGTGTAGTCTTCTTGCATGTGAC
TTATGTCCCTGCACAAGAAAAGAACTTCACAACCTGCTCCTGCCATTTGTCATGATGGAAAAGCA
CACTTTCCTCGTGAAGGTGTCTTTGTTTCAAATGGCACACACTGGTTTGTAAACACAAAGGAATT
TTTATGAACCACAAATCATTACTACAGACAACACATTTGTGTCTGGTAACTGTGATGTTGTAAT
AGGAATTGTCAACAACACAGTTTATGATCCTTTGCAACCTGAATTAGACTCATTCAAGGAGGAG
TTAGATAAATATTTTAAAGAATCATAACATCACCAGATGTTGATTTAGGTGACATCTCTGGCATT
ATGCTTACAGTTGTAACATTCAAAAAGAAATTGACCGCCTCAATGAGGTTGCCAAGAATTTAAA
TGAATCTCTCATCGATCTCCAAGAACTTGGAAAGTATGAGCAGTATATAAAATGGCCATGGTAC
ATTTGGCTAGGTTTTATAGCTGGCTTGATTGCCATAGTAATGGTGACAATTATGCTTTGCTGTA
TGACCAGTTGCTGTAGTTGTCTCAAGGGCTGTTGTTCTTGTGGATCCTGATGCAAATTTGATGA
AGACGACTCTGAGCCAGTGCTCAAAGGAGTCGCATTAGCTTACACATAAGCGGCCGCCCTGCAC
ACAGATTCTTCATGTTTTGAACCAAATCAACTTGTGATATCATGCTCAAAGAGGCCTTAATTATA
TTTTAATTTTTTAAATTTTTTATGAAAAAACTAACAGCAATCATGGAAGTCCACGATTTTGTAGACC
GACGAGTTCAATGATTTCAATGAAGATGACTATGCCACAAGAGAATTCCTGAATCCCGATGAGC
GCATGACGTACTTGAATCATGCTGATTACAATTTGAATTTCTCCTCTAATTAGTGATGATATTGA
CAATTTGATCAGGAAATTCATTTCTTCCGATTCCCTCGATGTGGGATAGTAAGAACTGGGAT
GGAGTTCTTGAGATGTTAACATCATGTCAAGCCAATCCCATCTCAACATCTCAGATGCATAAAT
GGATGGGAAGTTGGTTAATGTCTGATAATCATGATGCCAGTCAAGGGTATAGTTTTTTACATGA
AGTGGACAAAGAGGCAGAAATAACATTTGACGTGGTGGAGACCTTCATCCGCGGCTGGGGCAAC
AAACCAATTGAATACATCAAAAAGGAAAGATGGACTGACTCATTCAAATTTCTCGCTTATTTGT
GTCAAAGTTTTTTTACTTACACAAGTTGACATTAATCTTAAATGCTGTCTCTGAGGTGGAATT
GCTCAACTTGGCGAGGACTTTCAAAGGCAAAGTCAGAAGAAGTTCTCATGGAACGAACATATGC
AGGATTAGGGTTCCCAGCTTGGGTCTACTTTTTATTTTCAAGGATGGGCTTACTTCAAGAAAC
TTGATATTCTAATGGACCGAAACTTTCTGTTAATGGTCAAAGATGTGATTATAGGGAGGATGCA
AACGGTGCTATCCATGGTATGTAGAATAGACAACCTGTTCTCAGAGCAAGACATCTTCTCCCTT
CTAAATATCTACAGAATTGGAGATAAAATTTGTGGAGAGGCAGGGAAATTTTTCTTATGACTTGA
TTAAATGGTGGAAACCGATATGCAACTTGAAGCTGATGAAATTAGCAAGAGAATCAAGGCCTTT
AGTCCACAATTCCTCATTTTTGAAAATCATATCAAGACTTCTGTTGATGAAGGGGCAAAAATT
GACCGAGGTATAAGATTCCTCCATGATCAGATAATGAGTGTGAAAACAGTGGATCTCACACTGG
TGATTTATGGATCGTTTCCAGACATTTGGGGTTCATCCTTTTTATAGATTATTACTGGACTAGAAA

ATTACATTCCCAAGTAACCATGAAGAAAGATATTGATGTGTCATATGCAAAAGCACTTGCAAGT
GATTTAGCTCGGATTGTTCTATTTCAACAGTTCAATGATCATAAAAAGTGGTTCGTGAATGGAG
ACTTGCTCCCTCATGATCATCCCTTTAAAAGTCATGTTAAAGAAAATACATGGCCACAGCTGC
TCAAGTTCAAGATTTTGGAGATAAATGGCATGAACTTCCGCTGATTAAATGTTTTGAAATACCC
GACTTACTAGACCCATCGATAATATACTCTGACAAAAGTCATTCATGAATAGGTCAGAGGTGT
TGAAACATGTCCGAATGAATCCGAACACTCCTATCCCTAGTAAAAAGGTGTTGCAGACTATGTT
GGACACAAAGGCTACCAATTGGAAAGAATTTCTTAAAGAGATTGATGAGAAGGGCTTAGATGAT
GATGATCTAATTATTGGTCTTAAAGGAAAGGAGAGGGAAGTGAAGTTGGCAGGTAGATTTTTCT
CCCTAATGTCTTGGAAATTGCGAGAATACTTTGTAATTACCGAATATTTGATAAAGACTCATTT
CGTCCCTATGTTTAAAGGCTGACAATGGCGGACGATCTAACTGCAGTCATTA AAAAGATGTTA
GATTCCTCATCCGCCAAGGATTGAAGTCATATGAGGCAATTTGCATAGCCAATCACATTGATT
ACGAAAAATGGAATAACCACCAAAGGAAGTTATCAAACGGCCAGTGTTCGAGTTATGGGCCA
GTTCTTAGGTTATCCATCCTTAATCGAGAGAACTCATGAATTTTTTGAGAAAAGTCTTATATAC
TACAATGGAAGACCAGACTTGATGCGTGTTCACAACAACACACTGATCAATTC AACCTCCCAAC
GAGTTTGTGGCAAGGACAAGAGGGTGGACTGGAAGGTCTACGGCAAAAAGGATGGAGTATCCT
CAATCTACTGGTTATTCAAAGAGAGGCTAAAATCAGAAACACTGCTGTCAAAGTCTTGGCACAA
GGTGATAATCAAGTTATTTGCACACAGTATAAACGAAGAAAATCGAGAAACGTTGTAGAATTAC
AGGGTGCTCTCAATCAAATGGTTTCTAATAATGAGAAAATTATGACTGCAATCAAATAGGGAC
AGGGAAGTTAGGACTTTTGATAAATGACGATGAGACTATGCAATCTGCAGATTACTTGAATTAT
GGAAAAATACCGATTTTCCGTGGAGTGATTAGAGGGTTAGAGACCAAGAGATGGTCACGAGTGA
CTTGTGTCACCAATGACCAAATACCCACTTGTGCTAATAATGAGCTCAGTTTTCCACAAATGC
TCTCACCGTAGCTCATTTTTGCTGAGAACCCAATCAATGCCATGATACAGTACAATTATTTTTGGG
ACATTTGCTAGACTCTTGTGATGATGCATGATCCTGCTCTTCGTCAATCATTGTATGAAGTTC
AAGATAAGATACCGGGCTTGACACAGTTCTACTTTCAAATACGCCATGTTGTATTTGGACCCTTC
CATTGGAGGAGTGTGCGGCATGTCTTTGTCCAGTTTTTTGATTAGAGCCTTCCCAGATCCCGTA
ACAGAAAGTCTCTCATTCTGGAGATTCATCCATGTACATGCTCGAAGTGAGCATCTGAAGGAGA
TGAGTGCAGTATTTGGAAACCCCGAGATAGCCAAGTTTCGAATAACTCACATAGACAAGCTAGT
AGAAGATCCAACCTCTCTGAACATCGCTATGGGAATGAGTCCAGCGAACTTGTTAAAGACTGAG
GTTAAAAAATGCTTAATCGAATCAAGACAAACCATCAGGAACCAGGTGATTAAGGATGCAACCA
TATATTTGTATCATGAAGAGGATCGGCTCAGAAGTTTCTTATGGTCAATAAATCCTCTGTTCCC
TAGATTTTTAAGTGAATCAAATCAGGCACTTTTTTTGGGAGTCGCAGACGGGCTCATCAGTCTA
TTTTCAAATTTCTCGTACTATTCGGAACCTTTTAAAGAAAAGTATCATAGGGAATTGGATGATT
TGATTGTGAGGAGTGAGGTATCCTCTTTGACACATTTAGGGAACTTCATTTGAGAAGGGGATC
ATGTA AAAATGTGGACATGTT CAGTACTCATGCTGACACATTAAGATACAAATCCTGGGGCCGT
ACAGTTATTGGGACAACGTGACCCCATCCATTAGAAATGTTGGGTCCACAACATCGAAAAGAGA
CTCCTTGTGCACCATGTAACACATCAGGGTTCAATTATGTTTTCTGTGCATTGTCCAGACGGGAT
CCATGACGTCTTTAGTTCACGGGGACCATTGCCTGCTTATCTAGGGTCTAAAACATCTGAATCT
ACATCTATTTTTGCAGCCTTGGGAAAGGGAAAGCAAAGTCCCACTGATTA AAAAGAGCTACACGTC
TTAGAGATGCTATCTCTTGGTTTGTGTAACCCGACTCTAAACTAGCAATGACTATACTTTCTAA
CATCCACTCTTTAACAGGCGAAGAATGGACAAAAGGCAGCATGGGTTCAAAGAACAGGGTCT
GCCCTTCATAGGTTTTTCGACATCTCGGATGAGCCATGGTGGGTTTCGCATCTCAGAGCACTGCAG
CATTGACCAGGTTGATGGCAACTACAGACACCATGAGGGATCTGGGAGATCAGAATTTCGACTT
TTTATTCCAAGCAACGTTGCTCTATGCTCAAATTAACCACCACTGTTGCAAGAGACGGATGGATC
ACCAGTTGTACAGATCATTATCATATTGCCTGTAAGTCCTGTTTGAGACCCATAGAAGAGATCA
CCCTGGACTCAAGTATGGACTACACGCCCCAGATGTATCCCATGTGCTGAAGACATGGAGGAA
TGGGGAAGGTTTCGTGGGGACAAGAGATAAACAGATCTATCCTTTAGAAGGGAATTGGAAGAAT
TTAGCACCTGCTGAGCAATCCTATCAAGTCGGCAGATGTATAGGTTTTCTATATGGAGACTTGG

CGTATAGAAAATCTACTCATGCCGAGGACAGTTCTCTATTTCTCTATCTATAACAAGGTCGTAT
TAGAGGTCGAGGTTTCTTAAAAGGGTTGCTAGACGGATTAATGAGAGCAAGTTGCTGCCAAGTA
ATACACCGGAGAAGTCTGGCTCATTTGAAGAGGCCGGCCAACGCAGTGTACGGAGGTTTGATTT
ACTTGATTGATAAATTGAGTGTATCACCTCCATTCCTTTCTCTTACTAGATCAGGACCTATTAG
AGACGAATTAGAAACGATTTCCCAACAAGATCCCAACCTCCTATCCGACAAGCAACCGTGATATG
GGGTGATTGTCAGAAATTACTTCAAATACCAATGCCGTCTAATTGAAAAGGGAAAAATACAGAT
CACATTATTCACAATTATGGTTATTCTCAGATGTCTTATCCATAGACTTCATTGGACCATTCTC
TATTTCCACCACCCTCTTGCAAATCCTATAACAAGCCATTTTTATCTGGGAAAGATAAGAATGAG
TTGAGAGAGCTGGCAAATCTTTCTTCATTGCTAAGATCAGGAGAGGGGTGGGAAGACATACATG
TGAAATTCTTCACCAAGGACATATTATTGTGTCCAGAGGAAATCAGACATGCTTGCAAGTTCGG
GATTGCTAAGGATAATAATAAAGACATGAGCTATCCCCCTTGGGGAAGGGAATCCAGAGGGACA
ATTACAACAATCCCTGTTTATTATACGACCACCCTTACCCAAAGATGCTAGAGATGCCTCCAA
GAATCCAAAATCCCCTGCTGTCCGGAATCAGGTTGGGCCAATTACCAACTGGCGCTCATTATAA
AATTCCGGAGTATATTACATGGAATGGGAATCCATTACAGGGACTTCTTGAGTTGTGGAGACGGC
TCCGGAGGGATGACTGCTGCATTACTACGAGAAAATGTGCATAGCAGAGGAATATTCAATAGTC
TGTTAGAATTATCAGGGTCAGTCATGCGAGGCGCCTCTCCTGAGCCCCCAGTGCCCTAGAAAC
TTTAGGAGGAGATAAATCGAGATGTGTAAATGGTGAAACATGTTGGGAATATCCATCTGACTTA
TGTGACCCAAGGACTTGGGACTATTTCTCCGACTCAAAGCAGGCTTGGGGCTTCAAATTGATT
TAATTGTAATGGATATGGAAGTTCGGGATTCTTCTACTAGCCTGAAAATTGAGACGAATGTTAG
AAATTATGTGCACCGGATTTTGGATGAGCAAGGAGTTTTAATCTACAAGACTTATGGAACATAT
ATTTGTGAGAGCGAAAAGAATGCAGTAACAATCCTTGGTCCCATGTTCAAGACGGTCGACTTAG
TTCAAACAGAATTTAGTAGTTCTCAAACGTCTGAAGTATATATGGTATGTAAAGGTTTGAAGAA
ATTAATCGATGAACCCAATCCCGATTGGTCTTCCATCAATGAATCCTGGAAAAACCTGTACGCA
TTCCAGTCATCAGAACAGGAATTTGCCAGAGCAAAGAAGGTTAGTACATACTTTACCTTGACAG
GTATTTCCCTCCCAATTCATTCTGATCCTTTTTGTAAACATTGAGACTATGCTACAAATATTTCGG
AGTACCCACGGGTGTGTCTCATGCCGCTGCCTTAAAATCATCTGATAGACCTGCAGATTTATTG
ACCATTAGCCTTTTTTATATGGCGATTATATCGTATTATAACATCAATCATATCAGAGTAGGAC
CGATACCTCCGAACCCCCCATCAGATGGAATTGCACAAAATGTGGGGATCGCTATAACTGGTAT
AAGCTTTTGGCTGAGTTTGATGGAGAAAGACATTCCTACTATATCAACAGTGTTTGGCAGTTATC
CAGCAATCATTTCCGATTAGGTGGGAGGCTATTTAGTAAAAGGAGGATACAAGCAGAAGTGA
GTACTAGAGGTGATGGGCTCCCAAAAGATACCCGAATTTAGACTCCTTGGCCCCAATCGGGAA
CTGGATCAGATCTTTGGAATTGGTCCGAAACCAAGTTCGTCTAAATCCATTCAATAAGATCTTG
TTCAATCAGCTATGTCGTACAGTGGATAATCATTTGAAGTGGTCAAATTTGCGAAAAACACAG
GAATGATTGAATGGATCAATGGGCGAATTTCAAAGAAGACCGGTCTATACTGATGTTGAAGAG
TGACCTACATGAGGAAAACCTTTGGAGAGATTAATAAATCAGGAGGAGACTCCAACTTTAAGT
ATGAAAAAACTTTGATCCTTAAGACCCTCTTGTGGTTTTTATTTTTTATCTGGTTTTGTGGTC
TTCGT